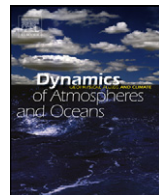




Contents lists available at ScienceDirect

## Dynamics of Atmospheres and Oceans

journal homepage: [www.elsevier.com/locate/dynatmoce](http://www.elsevier.com/locate/dynatmoce)



# Coastal Rapid Environmental Assessment in the Northern Adriatic Sea

Simona Simoncelli<sup>a,\*</sup>, Nadia Pinardi<sup>b</sup>, Paolo Oddo<sup>a</sup>, Arthur J. Mariano<sup>c</sup>, Giuseppe Montanari<sup>d</sup>, Attilio Rinaldi<sup>d</sup>, Marco Deserti<sup>d</sup>

<sup>a</sup> National Group of Operational Oceanography, Istituto Nazionale Geofisica e Vulcanologia, via Aldo Moro 44, 40128 Bologna, Italy

<sup>b</sup> Department of Physics, University of Bologna, Italy

<sup>c</sup> RSMAS University of Miami, USA

<sup>d</sup> ARPA Emilia Romagna, Italy

### ARTICLE INFO

#### *Article history:*

Received 14 October 2010

Received in revised form 15 April 2011

Accepted 19 April 2011

Available online 19 May 2011

#### *Keywords:*

Operational oceanography

Coastal observations

Forecasting system

Nesting

Adriatic

Optimal interpolation

### ABSTRACT

A new Coastal Rapid Environmental Assessment (CREA) methodology, based on an operational regional forecasting system and coastal monitoring networks of opportunity, has been developed and successfully applied to the Northern Adriatic Sea. The methodology aims at improving the initial condition estimates by combining operational coarse model fields with coastal observations to improve medium to short range predictability which is required by coastal zone and emergency management. The CREA modeling framework system consists of a high resolution,  $O(800\text{ m})$ , Adriatic SHELF model (ASHELF) nested into the Adriatic Forecasting System (AFS) at 2.2 km resolution. The CREA observational system is composed of coastal networks sampling the water column temperature and salinity between depths of 5 and 40 m.

The initialization technique blends the AFS fields with the available observations using a multi-input, multi-scale optimal interpolation technique and a spin-up period for the high resolution ASHELF model to dynamically adjust initial conditions from the coarser resolution AFS model. The high resolution spin up period has been investigated through a dedicated set of experiments and it was found that a week time is enough to have new energetic features in the model initial condition field estimates to be blended with observations.

\* Corresponding author.

E-mail address: [simona.simoncelli@bo.ingv.it](mailto:simona.simoncelli@bo.ingv.it) (S. Simoncelli).

Five CREA study cases have been analyzed for different months of the year, one per month from May to September 2003, chosen on the basis of the availability of the coastal observations for both model initialization and validation. The CREA 7-days forecasts show skill improvements in the coastal area salinity and temperature profiles, deriving from the blending and the spin-up period in the initialization methodology. The main conclusion is that forecasting in coastal areas by nesting necessitates of the observations to correct the coarse resolution model fields providing informations where parent and child model topographies mismatch. Results demonstrate the feasibility of a CREA strategy to support coastal zone management in line with recent operational oceanography developments.

© 2011 Elsevier B.V. All rights reserved.

## 1. Introduction

The concept of Marine Rapid Environmental Assessment (MREA) originates with the user needs to assess and predict as accurately as possible the ocean environmental state using all information available in an optimal way. Applications such as naval operations, emergency management at sea, marine environmental quality and ecosystem health are some of the user issues addressed by MREA. Robinson (1999) pioneered the field in the nineties and several of the original MREA concepts are at the basis of this study (Robinson, 2002; Ferreira-Coelho and Rixen, 2008).

Our system is called Coastal MREA (CREA) because it focuses on the coastal areas and addresses to the coastal protection and environmental management community. CREA novelty is represented by an initial condition (hereafter IC) taken from an operational model and local observations, named opportunity observations since they were not designed specifically for the forecasting activities.

CREA system is composed of an observational network, a numerical dynamical modeling system and a data assimilation scheme. The general goal is to assimilate observational data in the model IC in order to reduce the nowcast and forecast error and uncertainties. The advent of operational oceanography allowed to create the IC by downscaling coarse operational analyses into the higher resolution grid. However operational analyses are the least accurate in the coastal region due to the approximation of the coastline and bathymetry in the coarse resolution grid, the representation of river mouth positions and the effective runoff strength by the coarse grid. Thus, considering the coastal monitoring observations will allow to fill the gap between the parent and child model grids introducing new information.

This new CREA methodology has been applied to the Northern Adriatic Sea (see Fig. 1a), a landlocked basin located at the midlatitudes in the northernmost part of the Adriatic Sea, confined to the north by the Alps and laterally between the Apennine and the Balkans. The Northern Adriatic constitutes the shelf of the Adriatic basin that gently slopes towards the shelf break found at a nominal depth of 120 m. Its mean depth is 35 m with sandy and smooth coastal areas on its western side and an irregular eastern rocky shore, characterized by numerous channels and islands. The Northern Adriatic presents three main ambient density stratification regimes, widely described in Artegiani et al. (1997) and Jeffries and Lee (2007), with strong stratification from June through September and a weak stratification from December through March. A transitional stratification regime characterizes April, May, October and November. Fresh water input from many rivers is a primary forcing function on stratification with the Po River accounting for almost 80% of the total fresh water contribution to the Adriatic Sea. Wind is also a major forcing function and the regional winds are characterized by northeasterly Bora and sporadic southeasterly Scirocco winds.

Five CREA study cases will be discussed for the year 2003, from May to September, focusing the attention on three coastal areas of the Northern Adriatic Sea: Emilia-Romagna, Gulf of Trieste and Rovinj (Fig. 1b-d), where and when a coordinated network of monitoring stations, within the framework of ADRICOSM Project (Castellari et al., 2006), provided synchronous data for model initialization and forecast verification.

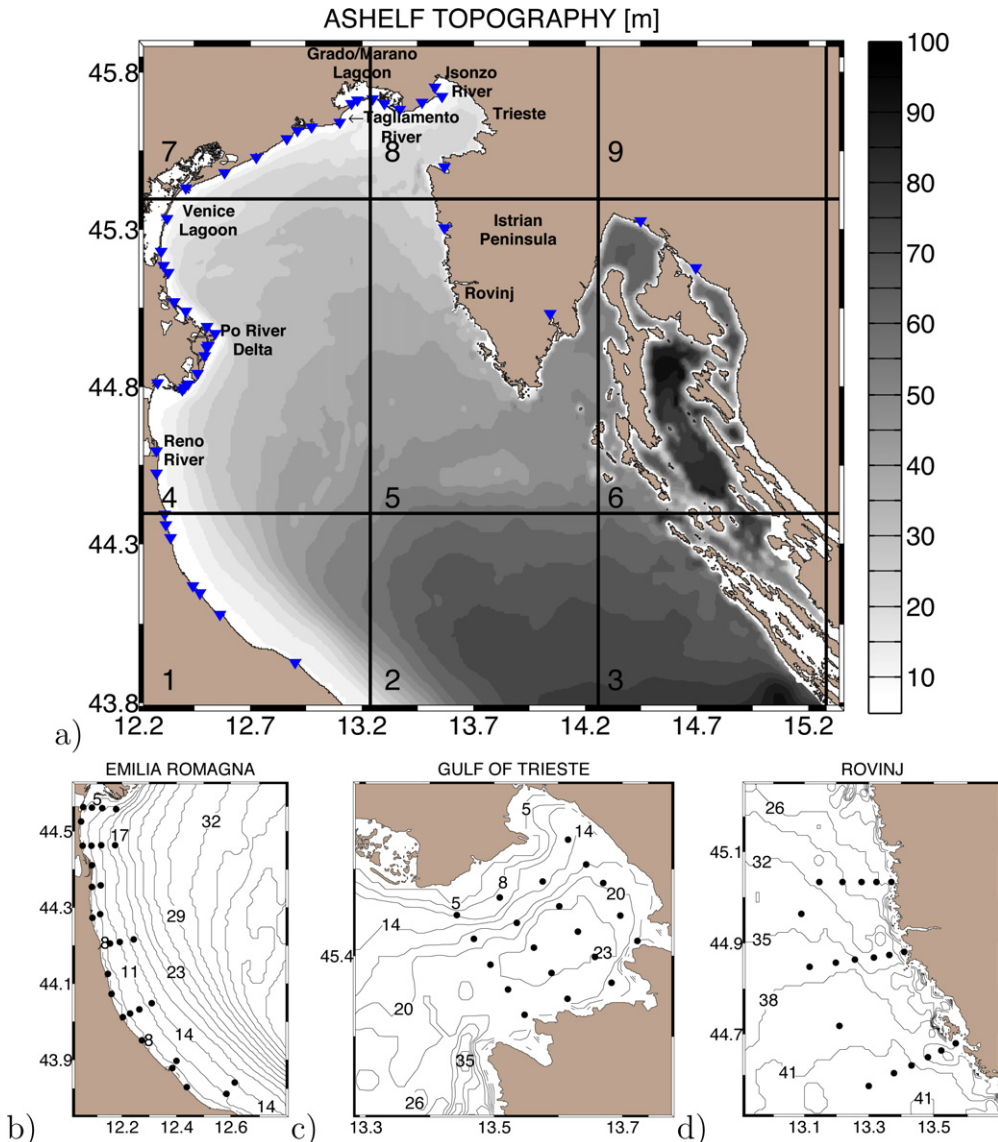


**Fig. 1.** (a) ASHELF model domain and topography in meters. Blue markers indicate river mouths locations. The domain has been subdivided in squares that will be used to define the Parameter Matrix for the Optimal Interpolation technique. Coastal topography and monitoring networks: (b) Emilia Romagna; (c) Gulf of Trieste and (d) Rovinj.

CREA modeling system consists of a high resolution ( $0.800\text{ m}$ ) Adriatic SHELF model (ASHELF) nested within the so-called Adriatic Forecasting System (AFS) which is operational since 2003 for the whole Adriatic (Oddo et al., 2006), recently upgraded to  $2.2\text{ km}$  resolution (Guarnieri et al., 2009). The nesting approach is necessary to both represent a more realistic coastal environment (Robinson, 1996; Pinardi et al., 2002) and to be able to explicitly resolve mesoscale features that the opportunity coastal observations capture. The first baroclinic Rossby radius of deformation in the Northern Adriatic Sea is about  $3\text{--}5\text{ km}$  (Paschini et al., 1993; Masina and Pinardi, 1994; Bergamasco and Gacic, 1996) thus ASHELF, rather than AFS, can explicitly resolve the mesoscale activities characterizing this

area. AFS analyses are going to be blended with the available coastal observations to produce optimal ASHELF ICs for CREA forecasts. The blending of the two data sets has been carried out with a multi-scale optimal interpolation technique (hereafter OI) developed by Mariano and Brown (1992).

Our objective is to demonstrate the feasibility and the quality of a CREA system for 7–8 days forecast in the near coastal areas of the Northern Adriatic Sea with respect to the already available AFS forecasts. Two atmospheric forcing data sets were considered with different spatial and temporal resolution for the purpose of understanding the sensitivity of the CREA approach to forcing resolution. Additionally, CREA sensitivity to the spin up time was analyzed to define the time required by ASHELF model to develop nonlinear scale features and the consequent effects on predictability.

The paper is organized as follows: a description of the modeling system is given in Section 2. Section 3 presents the observational networks of opportunity and the coastal data used to initialize and validate the CREA system. Section 4 explains the CREA methodology and the study cases. In Section 5 there is a description of the initialization and blending methods together with the IC spin up time evaluation. In Section 6 we discuss CREA results, while Section 7 contains a summary of our conclusions.

## 2. The Adriatic SHELF model

The CREA modeling system is ASHELF embedded in a hierarchy of two numerical models, the Mediterranean Forecasting System (MFS) model (Pinardi et al., 2003; Tonani et al., 2008) and the Adriatic Sea Forecasting System (AFS) model (Oddo et al., 2006). The Northern Adriatic nested model has been first implemented by Zavatarelli and Pinardi (2003) to study the climatological circulation proving that such nesting approach gives realistic climatological results.

The AFS produces daily 9 days forecasts (Guarnieri et al., 2009) of the main hydrodynamics state variables (currents, temperature, salinity, sea level) with a horizontal resolution of about 2.2 km and 31 vertical  $\sigma$  levels more compressed (logarithmic distribution) near the surface and the bottom, providing boundary conditions to ASHELF that models the Northern Adriatic basin (Fig. 1) with a horizontal resolution of 800 m and same vertical discretization. AFS daily mean fields are linearly interpolated in time on ASHELF lateral open boundary through a simple off-line, one way nesting approach.

Both AFS and ASHELF are a modified version of the Princeton Ocean Model (Blumberg and Mellor, 1987). The bathymetry in AFS has been modified by flattening the coastal area between the coastline and the 10 m depth contour, to have a minimum depth of 10m while preserving a realistic coastline. ASHELF instead introduces a new high resolution topography (Richard Signell personal communication from ADRIA03 field experiment in the Northern-Central Adriatic) which has been blended to the coarse resolution topography of AFS in a transitional layer of about 30 km from the lateral open boundary. The minimum depth of ASHELF is set to 5 m to further increase the realism of coastal zone representation.

Both ASHELF and AFS use the same Monotonic Upstream centered Scheme for Conservation Laws (MUSCL) for tracer advection (Estubier and Levy, 2000) in order to give a more realistic representation of horizontal and vertical gradients. An up-stream scheme, as in Oddo et al. (2009), has been applied close to the lateral open boundary to increase diffusivity avoiding numerical instabilities. Eddy viscosity is provided by the Smagorinsky (1993) parameterization and the diffusivity coefficients are obtained using the Prandtl number.

In order to reduce the truncation errors associated with the calculation of the baroclinic pressure gradient term in  $\sigma$  coordinates (Mellor et al., 1994, 1998) we subtracted  $\rho_{MEAN}$  from  $\rho$  in the equation for the total velocity.  $\rho_{MEAN}$  has been computed from AFS initial temperature and salinity fields vertically interpolated on 75 z levels, as it will be described in Section 5.1, and then area averaged over ASHELF domain.

ASHELF, as well as AFS, uses real fresh water input in the surface boundary condition for vertical velocity  $w$ :

$$w|_{z=\eta} = E - P - \frac{R}{A} \quad (1)$$

where  $\eta$  is the free surface elevation,  $E$  the evaporation rate [m/s],  $P$  the precipitation rate [m/s] and  $R$  the river volume discharge [ $m^3/s$ ], a non zero value only at the river mouth locations, divided by the area  $A$  of the corresponding horizontal grid cells. Considering no salt flux through the air-sea interface, the turbulent salt flux must exactly cancel out the advective salt flux. Thus the salt flux boundary condition becomes:

$$K_V \frac{\partial S}{\partial z} \Big|_{z=\eta} = (E - P)S_{surf} - \frac{R}{A}(S_{surf} - S_{river}) \quad (2)$$

where  $S_{surf}$  is the salinity at the sea surface and  $S_{river}$  is the river water salinity.

The open boundary condition for the meridional component of the barotropic velocity, normal to the boundary, uses the [Oddo and Pinardi \(2008\)](#) formulation of the Flather boundary condition. The tangential component is imposed to be identical to AFS. An advective condition is applied to tracers; at outflow points ASHELF tracers are advected through the boundary, otherwise the AFS values are prescribed. A southern radiation boundary condition, according to Orlanski's explicit scheme ([Orlanski, 1976](#)), is applied to the meridional component of the total velocity, normal to the lateral open boundary. The tangential component is imposed to be identical to AFS.

## 2.1. Incident solar radiation absorption

A difference between AFS and ASHELF is the solar radiation penetration parameterization for  $I$ , the downward irradiance. In the AFS model ([Pinardi et al., 2003; Oddo et al., 2005](#)),

$$\frac{I}{I_0} = Tr e^{z/\xi} \quad (3)$$

where  $I_0$  is the net incident irradiance at the surface,  $z$  the vertical coordinate,  $\xi$  is the attenuation length and  $Tr$  the transmission coefficient. A bimodal exponential parameterization for short wave radiation was introduced into the ASHELF model using the classification of [Jerlov \(1976\)](#) as interpreted by [Paulson and Simpson \(1977\)](#),

$$\frac{I(z)}{I_0} = Tr e^{z/\xi_1} + (1 - Tr) e^{z/\xi_2} \quad (4)$$

where,  $\xi_{1,2}$  are the attenuation lengths. The first exponential term characterizes the rapid light attenuation due to the absorption of the red end of the spectrum and  $\xi_1 = 1.5$  m while the second term represents the attenuation of blue-green light with  $\xi_2 = 14$  m. AFS assumes [Jerlov \(1976\)](#) water type IA while ASHELF assumes water type II, because its domain includes the area of largest river water influence and the water is on average more turbid.

## 2.2. River runoff parameterizations

River discharge data considered in ASHELF has been extracted from particular data sets described in detail in [Appendix A](#). The rivers are listed in [Table A.7](#) and their outlet location is shown in [Fig. 1a](#). This is a major difference with AFS which underlines the refinement that a nested model can introduce by increasing the degree of realism of the nowcast.

The Po daily discharge has been divided between the five main river mouths as a function of the runoff and values are listed in [Table A.8](#) of [Appendix A](#). [Fig. 2a](#) shows the daily Po River outflow for 2003 and the monthly climatology estimated for the time period 1995–2002. AFS also uses daily Po runoff values but distributed in a different way. Maximum river discharge usually occurs in May and between October and November but the whole year 2003 is characterized by very low Po River runoff due to the low precipitation and high temperatures recorded ([Olita et al., 2007; Grbec et al., 2007](#)).

In the salinity Eq. (2)  $S_{river}$  has been set to 15 psu since fresh water has mixed with seawater at the location of the river outlet points in the model grid.

The Po river waters have an imposed temperature signal in the latest ASHELF model and this is an important difference with AFS. [Fig. 2c](#) shows the Po river temperature data versus surface temperature sampled at a station of the Emilia Romagna monitoring network, where it is evident the faster warming

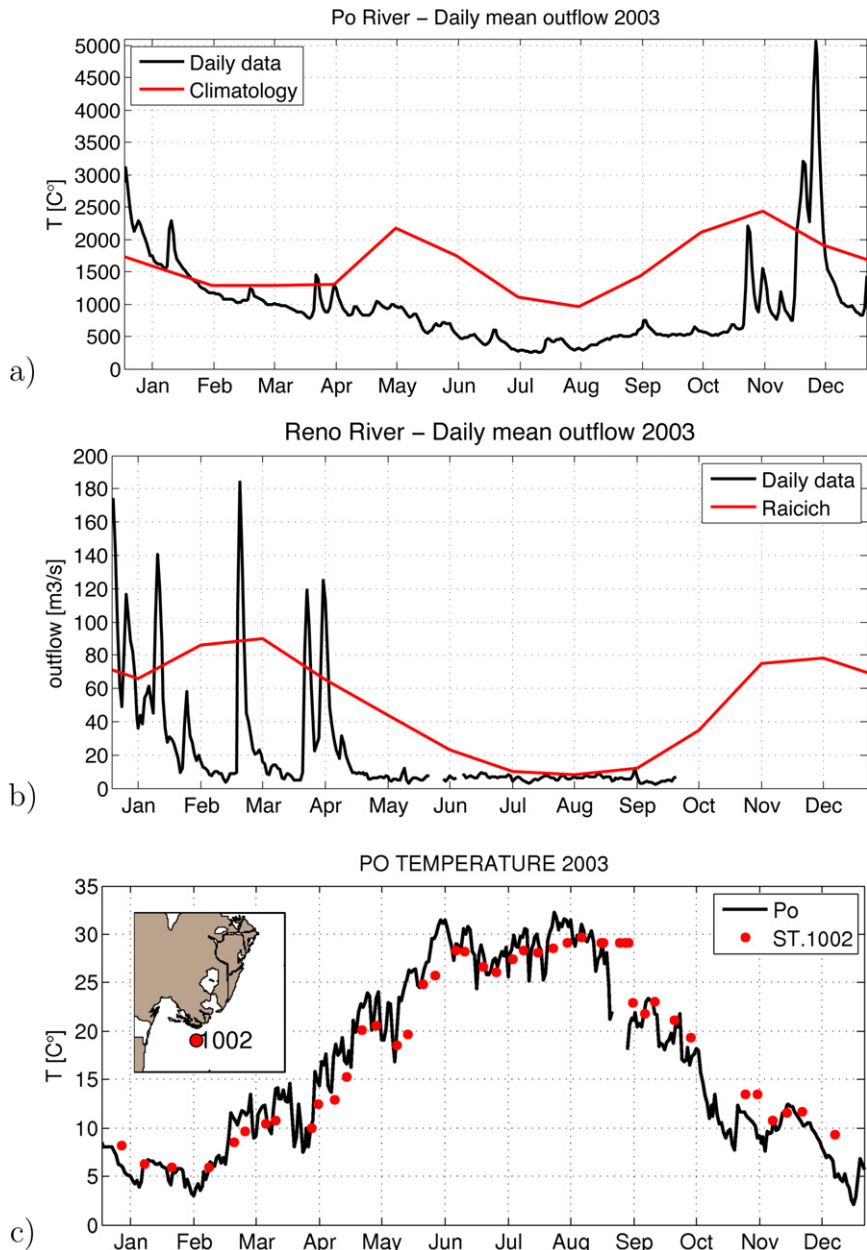


**Fig. 2.** (a) Po River daily mean outflow for the year 2003 and monthly climatology calculated for the time period 1995–2002. (b) Reno River daily outflow for 2003 and Raichich monthly climatology. (c) Po River daily temperature sampled at Canavella station and temperature sampled at station 1002 of Emilia Romagna coastal monitoring network, located just south the Po delta.

of Po river during spring time and its faster cooling during fall time. ASHELF model takes into account Po river temperature effect through a relaxation boundary condition at the Po river delta outlets,

$$K_V \frac{\partial T}{\partial z} \Big|_{z=\eta} = \frac{R}{A} (T_{surf} - T_{river}) \quad (5)$$

where  $T_{surf}$  is the model surface temperature,  $T_{river}$  is Po river daily mean temperature and  $R/A$ , the nudging term, is the river discharge rate defined at each Po river branch (Table A.8).

Reno is another major river for the Emilia-Romagna region (see Fig. 1); ASHELF uses daily outflow data which increases the runoff realism with respect to AFS climatological values, as shown in Fig. 2b.

### 2.3. Atmospheric forcing

Vertical surface boundary conditions are computed through standard bulk formulae parameterizations (Oddo et al., 2006). In ASHELF two different atmospheric data sets were used to calculate buoyancy and momentum fluxes: a coarse resolution data set from European Centre for Medium-Range Weather Forecasts (ECMWF) and a high resolution data set from Limited Area Model Italy (LAMI).

Signell et al. (2005) assessed the quality of surface winds derived from both ECMWF and LAMI over the Adriatic Sea finding that ECMWF fields underestimate the wind magnitude while LAMI exhibit a stronger amplitude winds together with a more realistic small scale spatial structure. However Signell et al. (2005) concluded that the smoother ECMWF field could be preferable to higher frequency LAMI in some real time applications due to LAMI higher phase error. Thus we decided to verify this result with our model set up. Moreover the use of ECMWF data also allows to verify ASHELF versus AFS model performance under the same forcing.

ECMWF provides data every 6 h at a space resolution of 0.5°. Air temperature, dew point temperature, mean sea level pressure, cloud cover and both wind components are the variables considered. Precipitation data have been extracted from Legates and Willmott (1990) global monthly climatology having a 0.5° horizontal resolution, accordingly to AFS (Oddo et al., 2006). ECMWF analyses were considered for our CREA hindcast exercises in 2003, to minimize ASHELF model uncertainty.

LAMI is the operational limited area model run by the Emilia Romagna regional meteorological agency, producing data every 3 h and a daily 72 h forecast on a 7 km grid. LAMI variables considered for surface fluxes computations are: air temperature, cloud fraction, relative humidity and wind components. LAMI precipitation data are introduced since they represent a crucial component of the fresh water flux on the daily time scale. LAMI daily forecasts, from 6 AM realization of day  $J$  to 3 AM of day  $J+1$ , were concatenated in a time series to be able to produce 8 days of forecast with maximum accuracy.

Fig. 3 shows air temperature time series and wind stick plot between May and September 2003 obtained calculating space averages over ASHELF domain from ECMWF and LAMI fields already interpolated on ASHELF grid. Land points have been masked before interpolation thus considering only sea points values. Time periods when CREA exercises were performed are highlighted in gray in Fig. 3a and c.

LAMI and ECMWF air temperatures (Fig. 3a) mostly exhibit a good correspondence of the general tendency indicating in May and June periods a warming tendency while July presents an abrupt cooling event on July 5th. August shows instead quite stable air temperature conditions. Between August and September air temperature drops of about 5 degrees and in September case air temperature oscillates and stabilizes around 20 °C. Diurnal cycles (Fig. 3b) are very different, with ECMWF exhibiting a larger amplitude diurnal cycle with maximum temperature at noon while LAMI maximum temperatures occur between 15 and 18 PM, which seems more realistic for the air over the ocean areas. ECMWF analyses in fact assimilate data from SYNOP stations over land using a structure function with an horizontal scale of the order of 1000 km (Anton Beljaars-ECMWF, personal communication). So the larger air diurnal cycle over land is affecting the ocean.

Wind stick plot (Fig. 3c) presents an overall good agreement between ECMWF and LAMI area averaged wind vectors over ASHELF domain since mean direction and timing look very similar, alternating

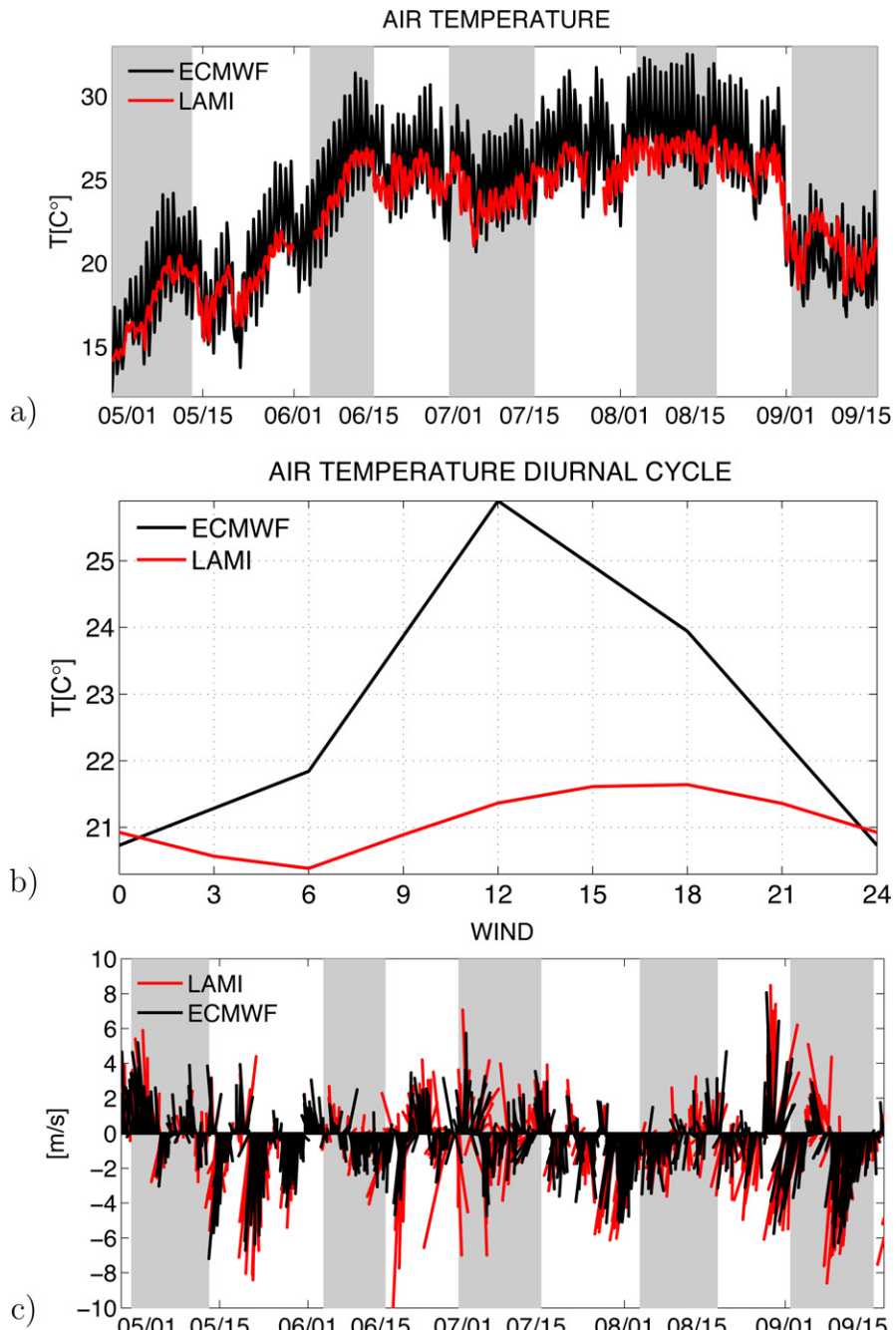


**Fig. 3.** ECMWF (black) and LAMI (red) data comparison from May to September 2003: (a) air temperature area averaged over ASHELF domain; (b) mean air temperature diurnal cycle calculated from the whole time period over ASHELF domain; (c) area averaged wind vectors. Gray areas highlight the time windows considered for CREA experiments.

**Table 1**

CTD data sets and collection periods. For Emilia Romagna region the second column indicates the number of stations monitored ( $N$ ). In the Gulf of Trieste and Rovinj coastal area the number of station monitored is constant and equal to 19.

Emilia Romagna		Gulf of Trieste	Rovinj area
Days	N		
May 05–06	29	May 05	May 05
May 12	23		May 13
June 09	17	June 09	June 09
June 16	12		June 16
July 07–08	29	July 07	July 07
July 15–16	29	July 14	July 15
August 11–12	29	August 11	August 11
August 18–19	29	August 18	August 19
September 09	8	September 09	September 09
September 17–18	29	September 17	September 15

intense Bora (northeasterly wind) and Scirocco (southeasterly wind) events with periods of wind stagnation in between. The average LAMI wind magnitude is larger than ECMWF, consistent with prior studies (Signell et al., 2005).

### 3. Observing networks

CREA introduces the notion of coastal monitoring networks of opportunity in order to ameliorate the nowcast and forecast in the coastal areas of the Northern Adriatic Sea. The three observational networks considered here are concentrated in the Emilia-Romagna, Gulf of Trieste, Rovinj coastal strips. The sampling arrays are displayed in Fig. 1b–d.

The first major coastal monitoring network in the whole Mediterranean Sea was established in the late seventies at Emilia-Romagna to study the environmental emergency related to eutrophication processes. This site has been maintained by the environmental protection agency (ARPA) to control water quality and the marine ecosystem health. The monitoring array (Fig. 1b) is made up of 29 stations situated along transects perpendicular to the coastline at distances of 500 m, 3, 6 and 10 km from the coastline carried out on a weekly basis on two consecutive days. The deepest stations sample to a depth of 15 m.

In the Gulf of Trieste bi-weekly (October 2002–March 2003) and weekly (April–September 2003) 1 day cruises (Celio et al., 2006) sampled 19 stations (Fig. 1c) providing an adequate spatial and temporal coverage of that region. The Gulf of Trieste is a semi-enclosed basin of about 30 km diameter with a complex topography with maximum depths of 26 m and influenced by the Isonzo river.

The third coastal network consists of three transects that are approximately perpendicular to the coast (Fig. 1d) with 19 stations. The maximum depth of 44 m is a few kilometers off the coast. Lyons et al. (2007) present a detailed analysis of all the CTD data collected in this area.

The CTD data used in our CREA experiments are listed in Table 1. They belong to five different periods between May and September 2003. All three regions have data at initialization time but in the Gulf of Trieste there are no data for verification in June and July cases. Emilia Romagna region has been monitored on a single day survey due to bad weather conditions on June 9 and September 9, therefore the corresponding CREA exercises used a reduced number of observations (indicated by  $N$  in Table 1) for the initial condition estimate. Furthermore CREA verification on May 12 and June 16 takes into account a reduced number of observations too.

### 4. CREA methodology and design of experiments

The experiments carried out to demonstrate the CREA methodology are illustrated in Fig. 4. Two important research issues in the CREA method are the IC estimate and the atmospheric forcing. The first issue is studied by evaluating three different initialization algorithms: the first, so-called IAFS (Interpolated AFS) is a simple interpolation–extrapolation procedure from the coarse to the higher

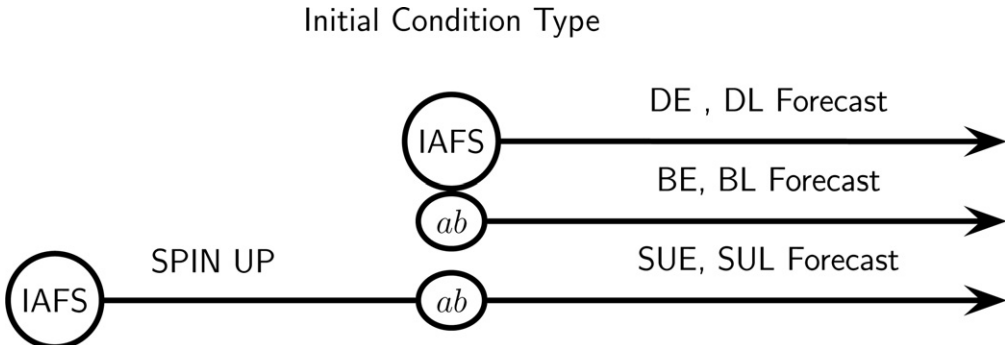


**Fig. 4.** CREA initialization and forecast experiments. IAFS indicates an ASHELF IC interpolated from AFS fields; DE and DL are the forecast experiments starting from it, the former forced by ECMWF and the latter by LAMI. ab indicates a blended IC, where AFS fields are melded with opportunity observations; BE and BL indicate the forecast experiments starting from it and forced by ECMWF or LAMI respectively. SUE, SUL forecasts start from ab IC that blends ASHELF fields with coastal observations after a preliminary spin up period initialized from IAFS; ECMWF and LAMI forcing are applied respectively.

resolution model grid. The second and third, called both *ab* (anisotropic blending), are IC fields obtained by melding the information from AFS with coastal observations or by melding ASHELF fields with coastal observations after a preliminary spin-up period that starts from IAFS.

The 7 days forecast period are also differentiated by the type of atmospheric forcing used (Fig. 4). The forecast is called *DE* if IAFS IC and ECMWF forcing are used, while it is called *DL* when IAFS IC and LAMI forcing are used. For the *ab* IC without spin-up the forecast is called *BE* or *BL* for ECMWF and LAMI forcing respectively. When a spin-up period is considered, the forecast is called *SUE* or *SUL* for ECMWF and LAMI forcing respectively. The spin up period length is explained in Section 5.4.

Five periods have been chosen to test the CREA methodology, between May and September 2003: (1) May 5–13; (2) June 9–16; (3) July 7–16; (4) August 11–19; (5) September 9–18. Five test scenarios demonstrate the CREA proof of concept since AFS fields provide varying initial skills and simultaneously ASHELF utilizes with very different atmospheric forcing conditions. Unfortunately CREA methodology could not be tested during the winter season because coastal observations were not available for model initialization and verification.

## 5. Initialization/blending method

### 5.1. Interpolation–extrapolation procedure

In this procedure, AFS daily mean fields of temperature, salinity and velocity have been first vertically interpolated from the AFS 31 vertical  $\sigma$  levels to 75 z levels and then re-interpolated onto the ASHELF 31 vertical  $\sigma$  levels. A zero gradient vertical boundary condition is applied at the surface, where the value at the first  $\sigma$  layer is associated with the zero depth level.

The new topography requires extrapolated values at ASHELF grid points where the bottom value was deeper than the AFS fields. Our approach takes into account the mean vertical water column structure in the Northern Adriatic Sea consisting of a strong seasonal cycle with a well-developed thermocline in spring and summer down to 30 m depth (Artegiani et al., 1997) in the open waters and at shallower depths in the near coastal zone. A threshold depth for the vertical extrapolation was set to 20 m for strong stratification conditions. Missing values deeper than 20 m have been generated from AFS using a zero gradient vertical boundary condition where the AFS bottom value is associated with the ASHELF deeper level.

Next the horizontal bilinear interpolation has been applied to vertically interpolated AFS fields and a new extrapolation procedure has been used to generate field values in regions near the coasts or shallower than 20m, where values are missing in AFS. Such procedure (also called sea-over-land) calculates average values from at least four neighboring points to the coasts and covers enough AFS

land points that it is now possible to interpolate to the high resolution grid. Lastly, the horizontally interpolated fields are then vertically interpolated on the ASHELF 31  $\sigma$  levels. This procedure assures to generate deep profile values preserving the vertical stratification.

### 5.2. Blending procedure

IAFS IC are corrected by coastal temperature and salinity observations through the multi-scale optimal interpolation (OI) technique developed by Mariano and Brown (1992). This scheme establishes a generalized approach to OI for non-stationary and dynamically heterogeneous fields via the “parameter matrix algorithm” (PM). This algorithm defines different correlation parameters in different regions of the analysis domain, named bins, and subtracts from observations a large scale trend, which are both fundamental issues in coastal areas where statistics and dynamics are far from being homogeneous and stationary.

One of the main assumptions in least square state estimation is that the statistics does not vary in the time interval and spatial domain considered and a practical approach to ensure this is to decompose the data field ( $T_o$ ) into three components,

$$T_o(x, y, t) = T_m(x, y, t) + T_e(x, y, t) + e_s(x, y, t) \quad (6)$$

where  $T_m$  is the contribution of the large scale or trend field,  $T_e$  is the natural field variability, important on the mesoscale or synoptic time scales, and  $e_s$  is the error due to the combined effect of sub-grid scale noise and measurement error. The choice of the trend field  $T_m$  should make the mean-squared value of  $T_e$  as small as possible and the  $T_e$  field homogeneous and isotropic. This method objectively interpolates just the deviations from the trend and the final field estimate is the sum of the large scale trend and the statistical interpolation of the small scale deviation field. Moreover for each interpolation grid location only few influential de-trended data points are considered and their local weighted average is also subtracted to remove local biases (Bretherton et al., 1976).

Another advantage of this technique is that different noise levels can be assigned to different data sets if, for example, they were sampled from different instruments. In our application the data are from both observations and from a numerical model. Random errors  $e_s$  have zero mean and it is assumed that they are not correlated with one another and with the observed variable but have known variance. The numerical value of the error is given as a fraction of total field variance.

A simplified version of the PM algorithm which considers only six parameters that vary in space and time is used here,

$$C(dx, dy, dt) = C(1) \left[ 1 - \left( \frac{dx}{C(2)} \right)^2 - \left( \frac{dy}{C(3)} \right)^2 \right] e^{-[(dx/C(4))^2 + (dy/C(5))^2 + (dt/C(6))^2]} \quad (7)$$

where

- $C(1)$  is the correlation at zero time and space lags and equals one minus the normalized (by the field variance) measurement variance (which includes a sub-grid scale component).  $C(1)$  is constant and equal to 0.98;
- $C(2)$  and  $C(3)$  are the zero crossing scales in the east–west and north–south direction respectively;
- $C(4)$  and  $C(5)$  are the spatial decay (e-folding) scales in the east–west and north–south direction respectively;
- $C(6)$  is the temporal decay scale.

This correlation function can be rotated in space by an arbitrary angle  $\theta$ .

The PM algorithm consists on dividing the interpolation grid and data domain in space–time bins, whose size depends on the correlation scales and how the correlation parameters change in space and time. Each bin contains one set of correlation parameters. The 9 space bins for our domain are depicted in Fig. 1a. The AFS field, vertically interpolated on pre-defined 75  $z$  levels applying the extrapolation procedure explained before, is the input in the OI. The other input is observed CTD data listed in Table 1, pre-processed as AFS field. Each variable, temperature and salinity, has been treated independently

**Table 2**

Heterogeneous Parameter Matrix (PM) defined for *ab* IC estimation. Each area, displayed in Fig. 1a and sorted by bin number, has its own set of correlation parameters. The other bins uses *ib* correlation parameters.

Area	Bin	C(2) (km)	C(3) (km)	C(4) (km)	C(5) (km)	$\theta$ ( $^{\circ}$ )
Emilia Romagna	1	89	111	56	70	315
Emilia Romagna	4	89	89	56	56	0
Rovinj	5	133	156	83	92	330
Gulf of Trieste	8	67	67	42	42	0
Others		45	45	28	28	0

with an univariate technique and analyzed on each pre-defined level assuming no vertical correlation. Velocities and surface elevation have been interpolated/extrapolated with the technique described in Section 5.1. Static stability was checked on the optimally interpolated fields and experiments conducted applying or not static stability correction recorded no differences on ASHELF temperature and salinity results. Surface elevation has been let to adjust by the model to the updated density field, based on Gabersek et al. (2007) that did not observe improvements on model predictability by damping spurious high frequency oscillations generated by model adjustment.

The trend field  $T_m$  has been estimated by least-square fitting a two dimensional bi-cubic spline surface (Mariano and Brown, 1992) over the entire domain considering both AFS and CTD data. The least square finite element splines have adjustable smoothness ( $\rho$ ) and tension ( $\tau$ ) parameters, allow variable data errors and use B-spline basis iterating with binary subdivision (Inoue, 1986). The smoothness parameter,  $\rho$ , controls the tradeoff between the fitness to the data and total smoothness: a small  $\rho(10^{-2})$  and a  $\tau(0.99)$  close to 1 give a smooth fit avoiding unrealistic values at the boundaries. This trend estimation procedure is advisable when the region is dynamically complicated; the computed salinity trends captured a permanent gradient characterized by highest salinity along the croatian coast, lowest values surrounding the Po River delta and the Italian coast, where fresh water discharge is maximum. Temperature trends, however, differ significantly within the upwelling front, coastal front and eddies, revealing a high variability over large-scale fields.

Normalized error of 0.16 and 0.03 are assigned to AFS fields and to coastal observations, respectively. The normalized error is multiplied by the standard deviation of the considered field variability yielding an error level that ranges for AFS temperature between 0.05 and 0.25  $^{\circ}$  C and for salinity between 0.18 and 0.25 psu. The noise level assigned to coastal observation corresponds to a measurement error ranging from 0.003 to 0.6 for both temperature and salinity that matches quite well sensors specifications, verified during ADRICOSM inter-calibration campaign (Celio et al., 2006). Six influential data are selected for each OI estimation location, that are the closest in space to the analysis point, without averaging. This procedure limits the computational time and minimizes the smoothing.

Correlation function parameters have been tuned to create the best data melding without smoothing out AFS field variability or high resolution coastal informations. The tuning started defining a homogeneous PM, i.e. the same parameters for all the areas (PM bins, see Fig. 1a), and an isotropic correlation function with correlation length scales,  $C(2)=C(3)=45$  km,  $C(4)=C(5)=28$  km, in agreement with the ones estimated by Jeffries and Lee (2007) for the Northern Adriatic sea from a large historical data set. The resulting field, named *ib* (isotropic blending), is shown in Figs. 5 and 6.

The correlation scales have been progressively enlarged up to  $C(2)$ ,  $C(3)=111$  km and  $C(4)$ ,  $C(5)=70$  km, assuming that the closer the blended IC field gets to observations, the better will be the forecast outcome starting from it. The tuning process highlighted the necessity to define different correlation scales in the three network of opportunity areas (PM bins, see Fig. 1a), owing to the different sampling schemes, as well as the local dynamics which strongly influence the final solution. The outcome is *ab* (anisotropic blending) IC field estimated using an heterogeneous PM, whose parameters, that vary from bin to bin, are listed in Table 2. In the southernmost zone of Emilia Romagna and Rovinj area (bin 1 and bin 5 in Table 2 and Fig. 1a) the correlation function is anisotropic and rotated of an angle  $\theta$  to align the longer correlation length scales,  $C(3)$ , with the local bathymetry. In the northernmost zone of Emilia Romagna and in the Gulf of Trieste (bin 4 and bin 8 in Table 2 and

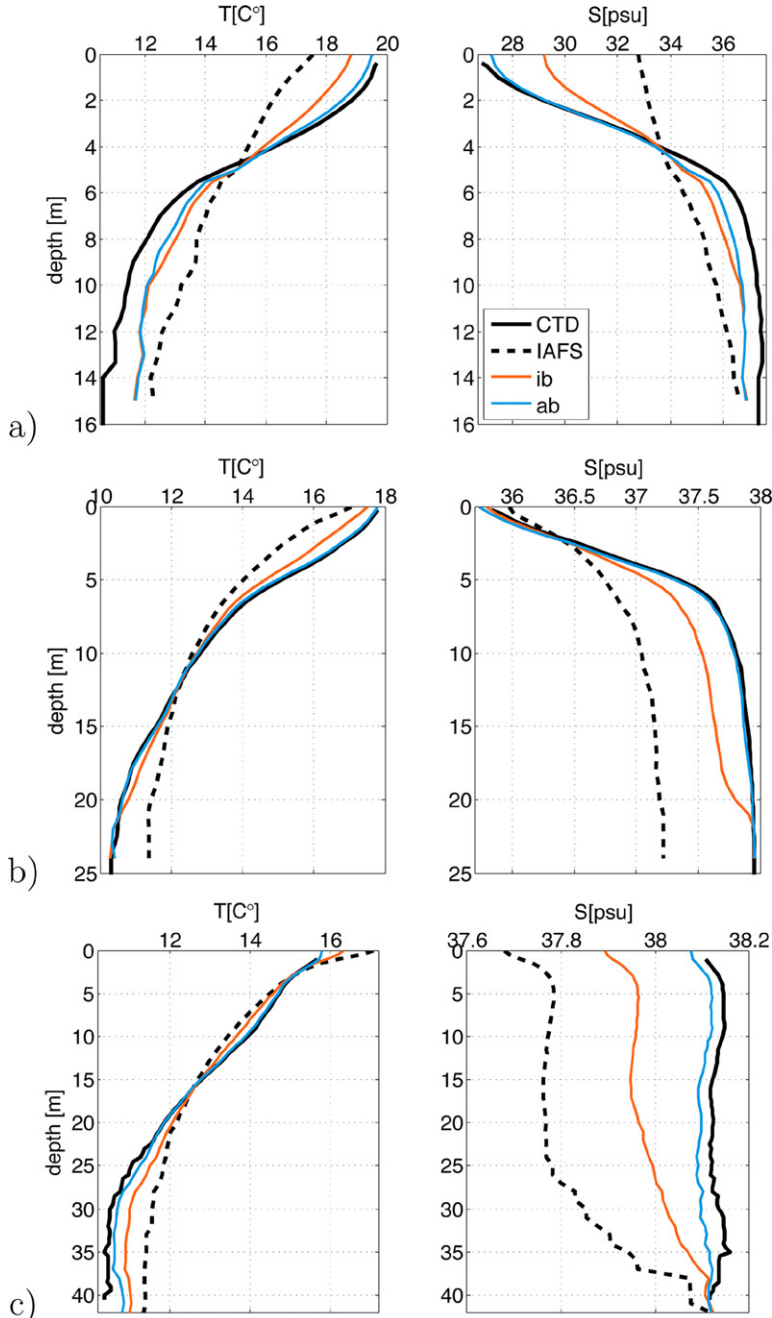


**Fig. 5.** Initial condition averaged profiles for May 5th: (a) Emilia Romagna; (b) Gulf of Trieste and (c) Rovinj. Black solid line represents observations. Dashed black line stands for the interpolated AFS daily mean fields (IAFS). *ib* is OI result from blending AFS with observations using an homogeneous PM and isotropic correlation scales ( $C(2)=C(3)=45$  km,  $C(4)=C(5)=28$  km). *ab* is OI result from blending AFS with observations using an heterogeneous PM and anisotropic correlation scales (Table 2). Profiles were obtained extracting synthetic profiles from the initial condition at each CTD location and then averaging them like observations.

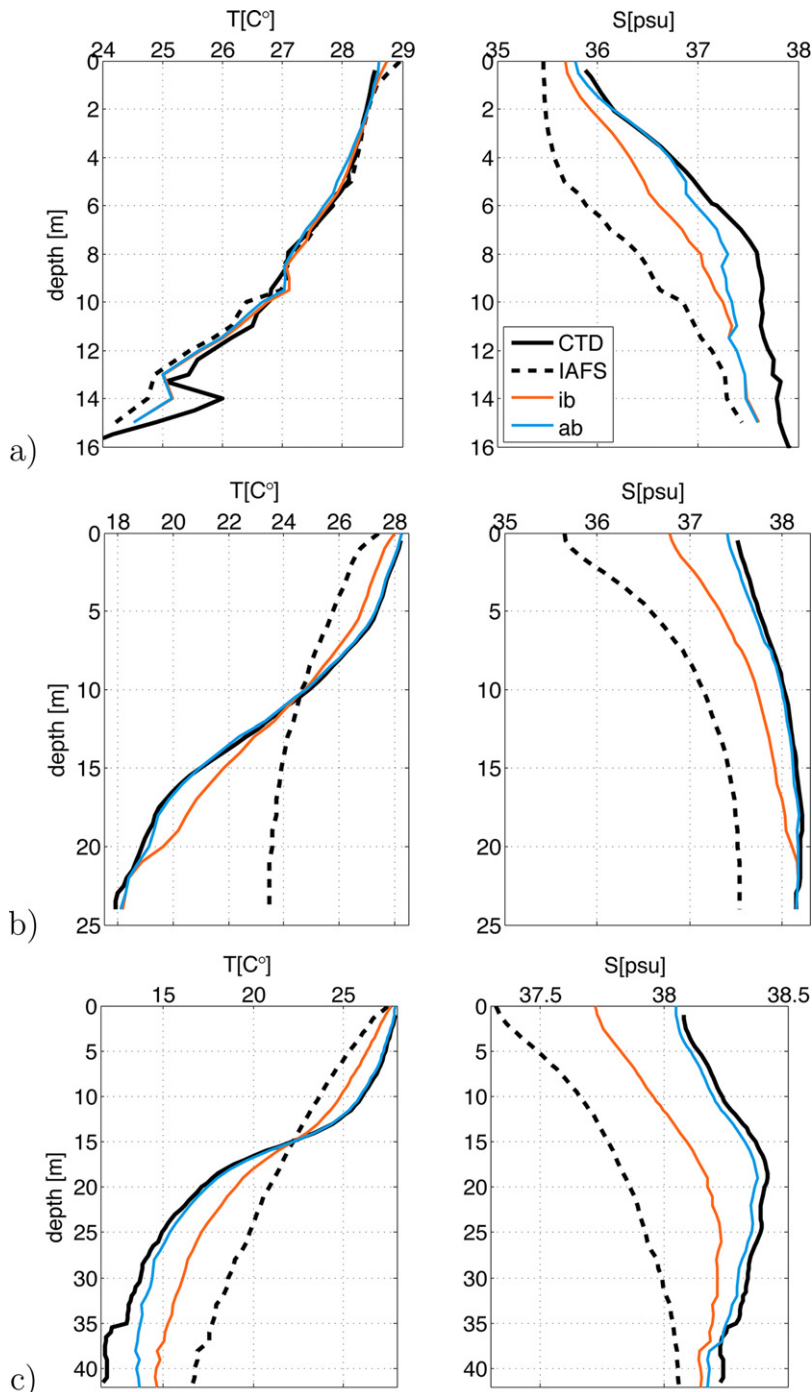


**Fig. 6.** Initial condition area averaged profiles for August 11th: (a) Emilia Romagna; (b) Gulf of Trieste and (c) Rovinj. Details in Fig. 5.

**Fig. 1a)** the correlation scales remain isotropic due to: the Po river plume influence on dynamics in the first zone; the effect of both local morphology and the sampling scheme in the second zone.

### 5.3. Blended initial condition evaluation

Figs. 5 and 6 display the outcome of both the interpolation–extrapolation procedure (IAFS) and the blending procedure for May and August cases. The presented profiles were obtained extracting synthetic profiles from the initial condition at each CTD location and then averaging them like observations.

The IAFS fields in Emilia Romagna area on May 5th (Fig. 5a) reveal unrealistic smooth temperature and salinity profiles with a surface temperature bias of the order of 2 °C and a surface salinity bias of about 6 psu. In the Gulf of Trieste (Fig. 5b) and Rovinj (Fig. 5c), IAFS generated profiles are too mixed and generally fresher with Rovinj salinity profiles showing a smaller misfit, less than 0.5 psu.

IAFS vertical stratification is again less pronounced in Trieste (Fig. 6b) and Rovinj (Fig. 6c) regions in August where a large positive bias characterizes the bottom layer. Average IAFS temperature agree with the observed value in Emilia Romagna (Fig. 6a), but IAFS salinity profiles in all three areas show an almost constant negative bias of about 1 psu.

The blending of AFS fields with coastal data using either *ib* or *ab* correlation parameters brings the blended IC profiles closer to the observations with *ab* producing the best agreement. *ab* is not as efficient in Emilia Romagna as in the other regions because the CTDs do not resolve the bottom layer and profile values are extrapolated from AFS as described above.

The validation of the blending technique in the Rovinj area has been carried out also using high-resolution satellite sea surface temperature (SST) data (Notarstefano et al., 2006). Fig. 7 shows the satellite SST image for May 5th at 6.52 AM (a), the IAFS SST field (b), the SST estimated from CTD observations only (c and d) and CTD observations and AFS fields (d and f) using different estimation parameters setting (*ib*, *ab*). The observed maps (c and e) are meant to show the effect of *ib* and *ab* correlation lengths when CDT only are considered: *ib* set up (c) defines a smaller area of influence of observations than *ab* set up (e). The blending procedure, weighting data according to their distance from the estimation location and the assigned noise level, corrects the AFS field (b) in a smaller area than that impacted by CTD only owing to the different resolution of the input fields. The satellite image (a) presents an upwelling front along the Istrian coastal area which is totally absent in the IAFS SST field (b). CTD data (c and d) confirm the presence of this cold front close to the coast. *ib* mapping (d) corrects AFS SST field in a small area surrounding each transect and the resulting field is patchy. *ab* mapping (f) uses a longer correlation scale parallel to the coastline and the resulting estimate is in better agreement with the satellite image. The best initialization method tested based on these comparisons is *ab* and it will be used hereafter to study the effects of observations blending for ICs.

Fig. 8 shows the *ab* ICs for the Emilia Romagna and for the Gulf of Trieste region versus the corresponding IAFS fields (a and d) and CTD observed maps (b and e), to show how both data set are blended according to the corresponding parameters (Table 2). The *ab* temperature fields (c and f), confirm how the blending procedure reduces the area of observational impact as consequence of the different resolution of the input data. IAFS SST (a and d) is colder than observations and *ab* fields (c and f) are closer to observations in the coastal areas. Po River fresh water warms up faster than the near coastal surface layer in Emilia Romagna zone where *ab* generates a large temperature gradient parallel to the shoreline (c). Inside the Gulf of Trieste IAFS (d) presents a cold plume in front of the Isonzo River outlet which is absent in the observations (e) while warmer water characterizes the southern-central area. The observed temperature is even higher in the lower zone (e). *ab* (f) smooths the cold plume and creates a warm water pool in the deepest part of the basin.

### 5.4. Initial condition spin up

The spin-up time is defined here as the time necessary by the high resolution ocean model to reach a steady state value for the volume average kinetic energy starting from initial and lateral boundary conditions interpolated from the parent model. Gabersek et al. (2007) reviewing different spin-up strategies, defined this approach a “cold model start”. A dedicated experiment has been performed

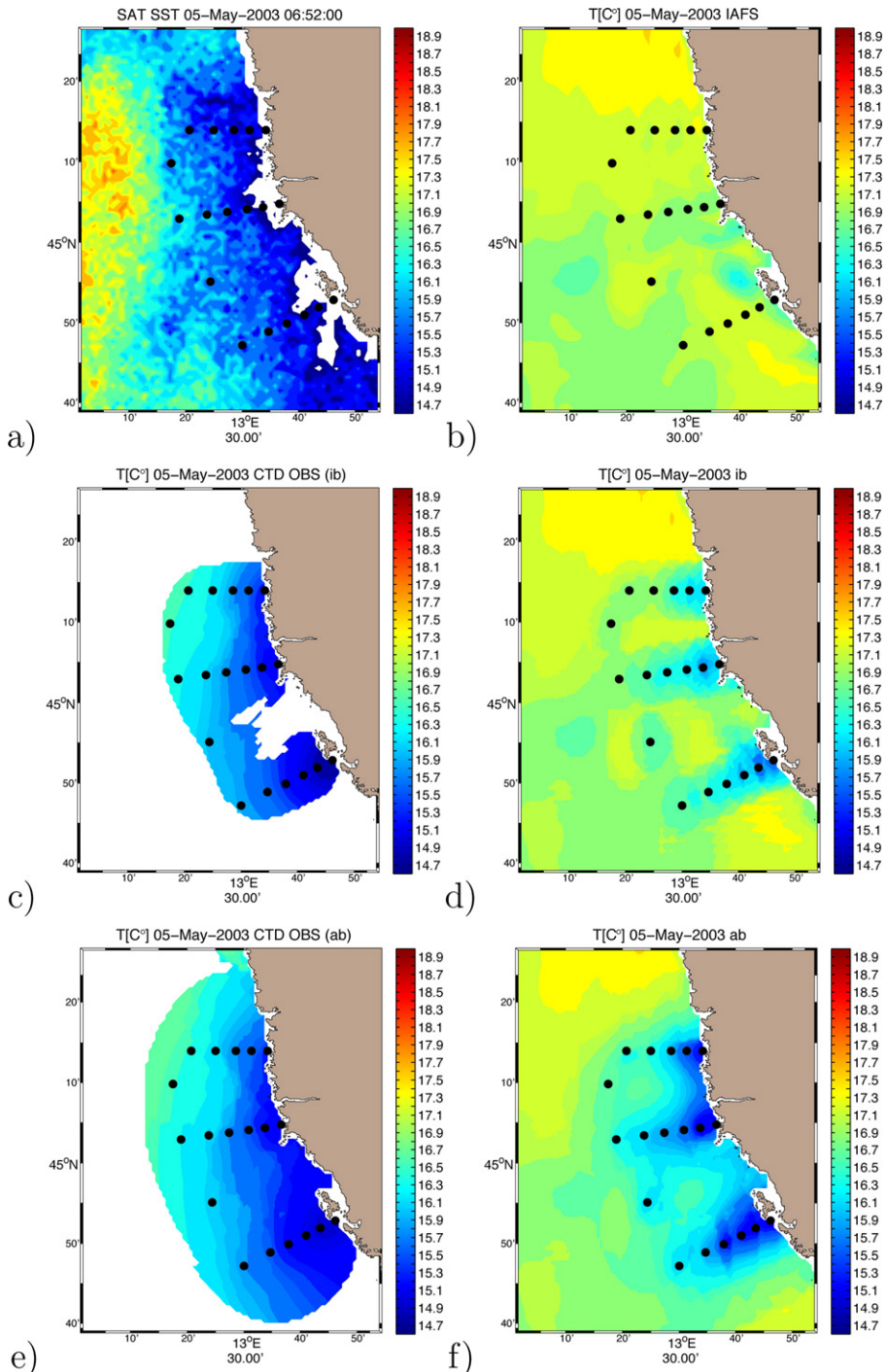


**Fig. 7.** SST fields on May 5th for the Rovinj coastal area: (a) Satellite high resolution SST image; (b) IAFS SST field; (c) *ib* observed SST; (d) *ib* blended SST; (e) *ab* observed SST; (f) *ab* blended SST. (SST fields have been masked for mapping error greater than 30%).

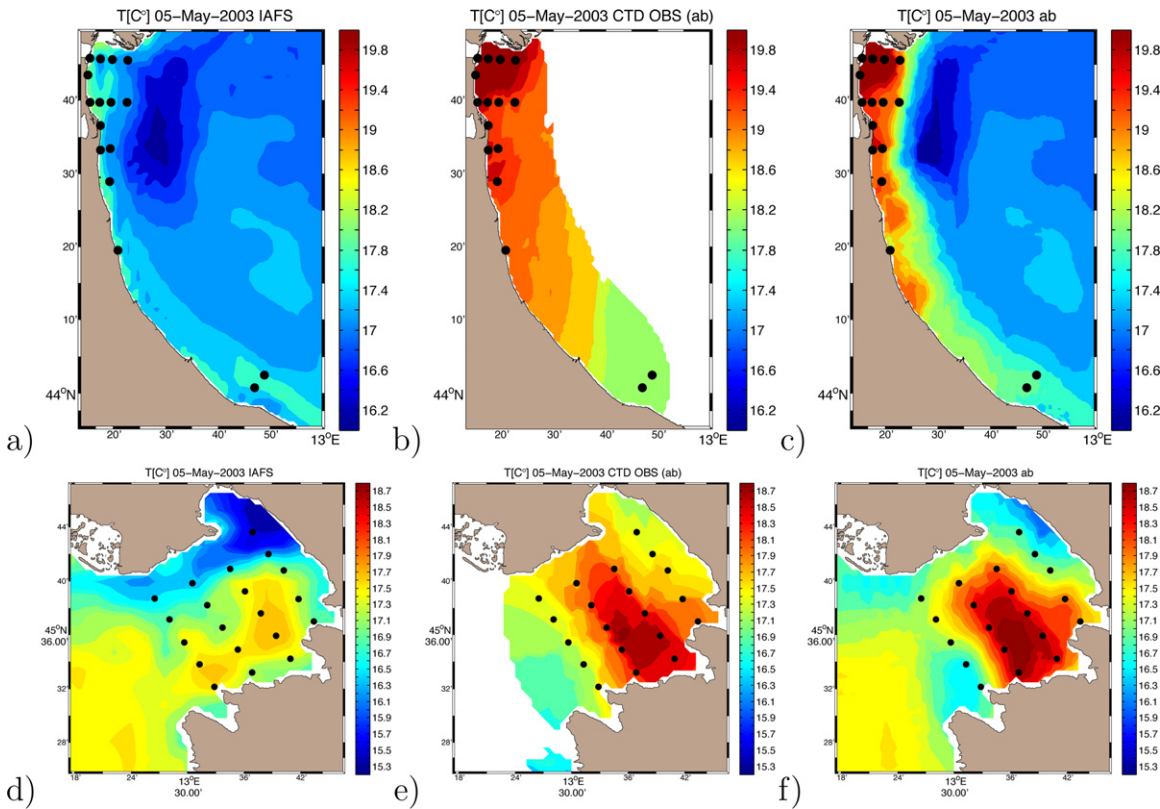


**Fig. 8.** SST fields on May 5th for the Emilia Romagna coastal area (a–c) and the Gulf of Trieste region (d–f). (a–d) IAFS SST; (b–e) ab observed SST; (c–f) ab blended SST. (SST fields have been masked for mapping error greater than 30%).

fixing a target IC at day ( $J$ ) and running several experiments starting from  $J - 1, J - 2, \dots, J - 21$  days before the target day. The total kinetic energy (TKE) of the ASHELF flow field is then calculated for the 21 experiments by

$$TKE = \frac{1}{VOL} \int_V \frac{(u^2 + v^2)}{2} dx dy dz \quad (8)$$

at the target day  $J$ . The spin-up experiment is repeated for the target day of May 5th and August 11th in order to check seasonal dependencies.

**Fig. 9a** illustrates the ratio between ASHELF and AFS TKE at day  $J$  as a function of the spin-up period length. Initializing ASHELF at  $J - 1$  results in a TKE ratio value smaller than one, indicating that the first few days adjustment of IAFS is dissipative and then advective dynamics starts to change the flow field only after 2–3 days. In fact ASHELF rises to AFS TKE values at  $J$  after at least two days of integration and then it exceeds it and reaches a plateau starting from the experiments initialized at  $J - 7$  and  $J - 9$ . The two curves adjust to different energy levels, with the highest ratio of approximately 1.5 for the 11th of August, due to both the external forcing regime and to the increased mesoscale activity which characterizes the Adriatic during summertime. The model behavior related to the spin-up time is further investigated by comparing model temperature and salinity to observations in the three coastal areas using root-mean-square-error statistics with the aim to understand if model results change as function of spin up time. Area-averaged RMSE,

$$RMSE = \sqrt{\frac{\sum_{ij} (\theta_{i,j}^m - \theta_{i,j}^o)^2}{N}} \quad (9)$$

have been calculated by extracting simulated ASHELF profiles at the space/time CTD locations, and the results for Emilia Romagna coastal area on target day, May 5th, are plotted in **Fig. 9b** and c. An exponential reduction of RMSE for both ASHELF temperature (b) and salinity (c) occurs if ASHELF is initialized 7–8 days in advance of the target day. Temperature improvement after a week of spin up is on the order of 0.3 °C or 13% while salinity improvement is about 0.8 psu or 19.5%, suggesting that 1 week of model spin up might improve our simulation in Emilia Romagna coastal area on the considered target day.

Salinity response in the other coastal areas and on the summer target day is similar with a progressive reduction of RMSE as function of model spin up time of about 11% after 7 days and 15% after 14 days. Temperature response in the other cases does not look sensitive to the spin up time since its RMSE settles around the initial RMSE value determined by the IAFS IC, indicating no particular relationship between day of spin up and temperature RMSE skill.

The spin-up of 7 days will increase the salinity IC realism and quality with respect to observations, while it will positively affect temperature IC only in one case. We conclude then that a spin-up period of 1 week for the IC is likely to augment the skill of the forecast allowing for both river influence and resolved mesoscale dynamics to evolve in the correct direction. However we believe also that the spin-up period is extremely sensitive to specific conditions and it should be considered as a tunable parameter for each specific case.

## 6. Results

CREA experiments, shown in **Fig. 4** are now evaluated in terms of 7–8 days forecast skill. Data used for validation are: (1) Satellite sea surface temperature (SST) (Notarstefano et al., 2006) on a 1.2 km horizontal resolution grid and (2) CTD from the three coastal networks at day  $J + 7/8$  (listed in **Table 1**). The CREA skill scores and their total improvement related to AFS reference skill, are listed in **Table 3** for SST data validation, in **Table 4** for the Emilia Romagna region, in **Table 5** for the Gulf of Trieste and in **Table 6** for the Rovinj coastal area. The main objective of the developed CREA methodology is to reduce the uncertainties of the existing AFS operational system, therefore CREA results are presented as averaged percentage of RMSE reduction with respect to AFS, called hereafter total gain (**Tables 3–6**).

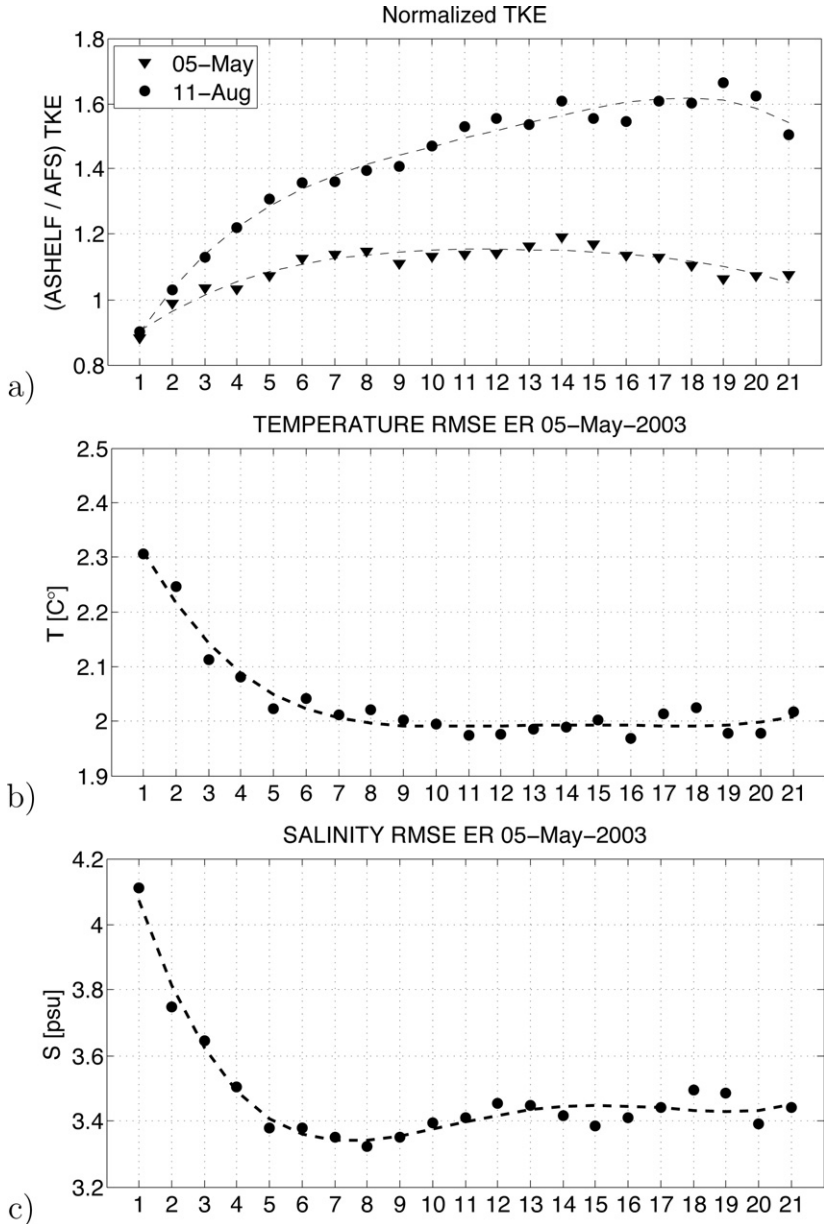


**Fig. 9.** (a) Total Kinetic Energy ratio between ASHELF and AFS calculated on target IC days, May 5th and August 11th as a function of spin up time. (b) Temperature and (c) Salinity RMSE calculated on day May 5th for the Emilia Romagna region as a function of spin up time. The abscissae indicate the days of integration from initialization.

### 6.1. Satellite SST validation

SST validation aims to evaluate ASHELF model performance over the entire domain and over the whole period of forecast and verify the impact of the new light absorption parameterization first under the same AFS atmospheric forcing (ECMWF) and second when a higher resolution forcing (LAMI)

**Table 3**

RMSE calculated from available SST images during the CREA experiments. Last line contains the different ASHELF total improvements in percentage relative to AFS RMSE.

	AFS	DE	DL	BE	BL	SUE	SUL
May	2.13	1.34	1.27	1.33	1.26	1.41	1.32
June	1.52	1.59	1.64	1.54	1.60	1.34	1.40
July	0.86	0.92	1.45	0.87	1.42	0.82	1.36
August	1.00	0.90	1.28	0.88	1.24	0.85	1.20
September	1.05	1.01	1.03	0.97	1.03	1.00	1.06
Total gain %		8	-13	12	-10	14	-7

**Table 4**

Temperature and Salinity RMSE for CREA forecast in the Emilia Romagna coastal area when observations were available for validation. Last line contains total temperature and salinity gain expressed as RMSE reduction or increase in percentage relative to AFS.

	AFS	DE	DL	BE	BL	SUE	SUL
Temperature [°C]							
May	2.25	2.05	2.03	1.86	1.90	1.86	1.93
June	2.55	2.13	2.56	2.11	2.46	2.16	2.61
July	1.26	1.11	1.26	1.13	1.17	1.15	1.15
August	0.85	0.66	0.58	0.63	0.66	0.52	0.61
September	0.55	0.46	0.43	0.44	0.44	0.39	0.42
Total gain %		15	13	18	14	22	15
Salinity [psu]							
May	3.42	3.21	3.15	3.02	3.02	2.97	3.00
June	0.56	0.55	0.68	0.53	0.63	0.58	0.68
July	1.65	1.48	1.52	1.20	1.25	1.25	1.28
August	1.11	1.01	1.09	0.95	0.88	0.90	0.91
September	1.46	1.37	1.32	1.33	1.34	1.12	1.21
Total gain %		6	1	14	11	15	10

is applied. Obtained model SST fields were not expected to improve with coastal data assimilation considering that CTD observations sample the surface only at 0.5–1 m depth and during summer this depth may have a temperature value considerably different from SST satellite data.

The RMSE for each day of the forecast using the high-resolution SST images for truth are examined next. Since the satellite SST observations are cloud masked, only maps with more than the 50% of available points inside ASHELF domain have been selected. Table 3 summarizes the RMSEs computed considering all the images available during each CREA forecast, while Fig. 10 shows their temporal

**Table 5**

Temperature and Salinity RMSE for CREA forecast in the Gulf of Trieste when observations were available for validation. Last line contains total temperature and salinity gain expressed as RMSE reduction or increase in percentage relative to AFS.

	AFS	DE	DL	BE	BL	SUL	SUE
Temperature [°C]							
July	2.08	1.99	2.26	1.84	1.97	1.88	2.1
August	2.35	2.00	1.93	1.55	1.34	1.58	1.38
September	0.94	1.04	0.93	0.46	0.36	0.53	0.45
Total gain %		3	3	32	37	29	31
Salinity [psu]							
July	2.09	1.77	1.43	1.17	0.74	1.17	0.85
August	1.66	1.34	0.98	0.88	0.61	0.83	0.49
September	0.82	0.63	0.50	0.47	0.21	0.44	0.27
Total gain %		19	38	45	68	47	66

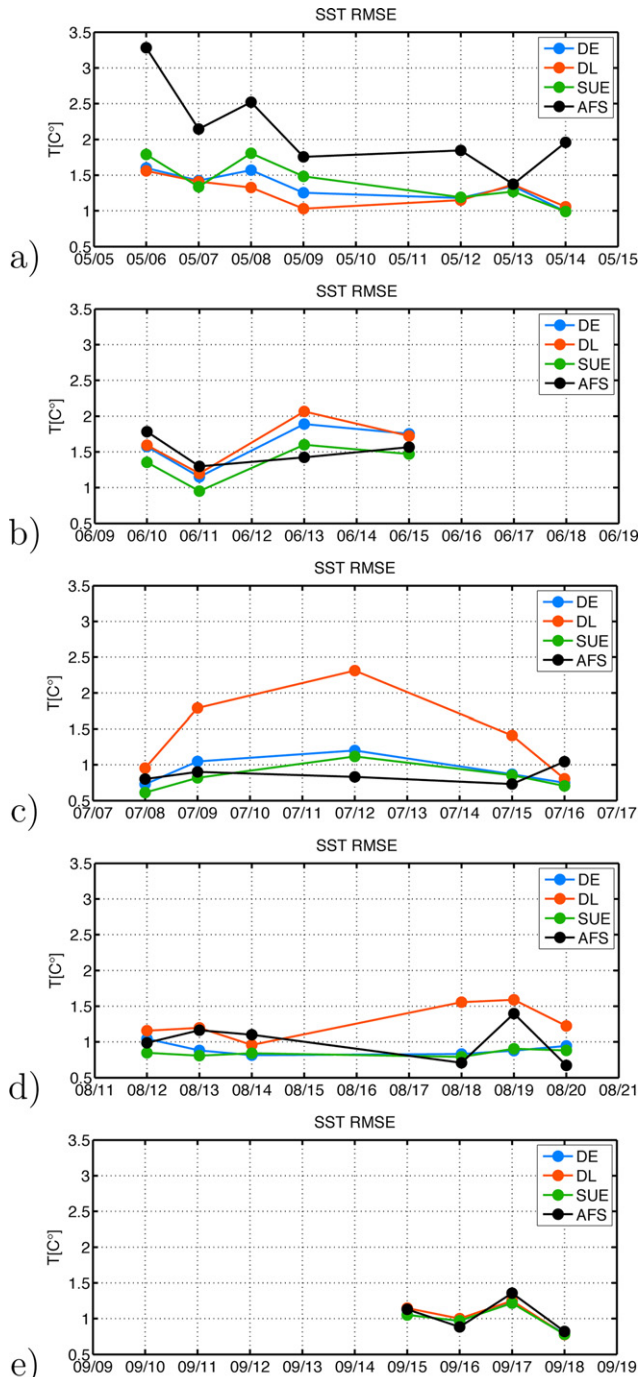


**Fig. 10.** SST RMSE time series calculated between satellite high resolution SST images and AFS daily mean SST field (black line), ASHELF forced by ECMWF (DE orange line), ASHELF forced by LAMI (DL blue line) and ASHELF forced by ECMWF after a week spin up period (SUE green line): (a) May; (b) June; (c) July; (d) August and (e) September.

**Table 6**

Temperature and Salinity RMSE for CREA forecast in Rovinj coastal area when observations were available for validation. Last line contains total temperature and salinity gain expressed as RMSE reduction or increase in percentage relative to AFS.

	AFS	DE	DL	BE	BL	SUE	SUL
Temperature [°C]							
May	1.00	0.90	0.93	0.78	0.77	0.75	0.74
June	1.86	1.72	1.65	1.35	1.44	1.38	1.38
July	2.58	2.54	2.44	1.8	2.17	2.03	2.20
August	3.43	3.36	3.47	2.30	2.55	2.21	2.57
September	3.10	3.05	2.77	2.08	1.97	2.07	1.99
Total gain %		5	7	29	25	28	26
Salinity [psu]							
May	0.49	0.48	0.45	0.36	0.33	0.28	0.26
June	0.51	0.48	0.53	0.32	0.38	0.33	0.40
July	0.53	0.55	0.57	0.49	0.52	0.53	0.54
August	0.80	0.80	0.63	0.60	0.46	0.44	0.38
September	0.51	0.49	0.41	0.35	0.31	0.36	0.31
Total gain %		2	7	26	28	30	32

evolution. In Fig. 10 only DE, DL and SUE cases are compared to AFS since blending did not significantly enhance, as expected, DE and DL SST results (Table 3) while the spin up approach improves them of an additional 6% independently from the atmospheric forcing utilized.

In May CREA methodology largely improves AFS score reducing the RMSE of a 38–40% (Fig. 10a), independently from the atmospheric forcing applied but without any substantial advantage from a preliminary spin up period run. ASHELF corrects the big AFS positive bias, giving a mean RMSE of about 1.3 °C. DE mean bias is 0.4 °C, DL is 0.1 °C (not shown). The RMSE reduction is presumably due to the new light penetration parameterization which allows the red component of the spectrum to penetrate within the first 1.5 m layer instead of being absorbed only at the surface and to the smaller LAMI air temperature diurnal excursion highlighted in Fig. 3b.

In June DE and DL slightly worsen AFS result, but in this case adding a spin up reduces AFS RMSE in the first days of forecast with a gain of about 12% (SUE in Fig. 10b). These results do not depend on the atmospheric forcing applied.

In July, as in June (Fig. 10c) DE slightly worsens AFS result, but when a spin up is used (SUE) the result improves in the first 2 days of forecast. On contrary when LAMI forcing is applied (DL) SST field fast degenerates, reaching 2.4 °C RMSE on July 12th, but getting back to DE and SUE skills on July 16th. DL presents on July 12th a 2 °C negative bias, double of the corresponding SUE estimate, indicating an abrupt surface cooling.

In August (Fig. 10d) CREA DE has better skill scores than AFS by a 10% and SUE RMSE further reduces respect to DE in the early days of forecast. DL presents higher RMSE values than AFS as in July and again, when LAMI forcing is applied, ASHELF negative bias ( $DL = 1^{\circ}\text{C}$ ) strongly increases. In both cases this is due to a very different cloud cover field in the two forcing data sets and a better estimation of it in the ECMWF analyses. LAMI cloud cover on July 7–8 and August 17–18 is much higher than ECMWF compromising the solar radiation component of the total heat flux, causing the SST cooling.

In September (Fig. 10e) all CREA implementations present approximately the same AFS skill score, without any additional gain from a spin up run, probably hidden because of the satellite data availability only in the last day of forecast.

When ECMWF forcing is applied (DE) the new light penetration parameterization brings about an 8% improvement on SST scores with respect to AFS reducing its positive characteristic bias. LAMI forcing determines a cooling on SST because of an overestimation of the total cloud cover, whose effect sums up with the new light absorption parameterization effect, worsening the result with respect to AFS performance. A preliminary spin up period can, in most of the cases (Fig. 10b–d), improve CREA results in the first days of forecast due to the combined effect of the coastal data assimilation and the

development of new features allowed by the enhanced ASHELF horizontal resolution, bringing about a 14% total gain (SUE).

## 6.2. CTD validation

ASHELF validation with coastal observations is presented in Figs. 11–13 for the Emilia Romagna region, the Gulf of Trieste and the Rovinj coastal area respectively, where vertical profiles have been computed extracting synthetic profiles from AFS and ASHELF models outputs at CTD space–time locations and then averaging them.

In the Emilia Romagna region (Table 4) CREA downscaling approach leads to a temperature gain ranging from 15%(DE) to 13%(DL) that slightly ameliorates to 18%(BE) assimilating coastal observations and to 22%(SUE) adding a week spin up period, but only if ECMWF forcing is used. Salinity skill scores show a 6% total gain in the downwelling approach (DE) which further increases to 14–15% in BE and SUE implementations. When LAMI atmospheric forcing is considered both temperature and salinity produce on average worst results. In Fig. 11 only ASHELF cases forced by ECMWF (DE, BE, SUE) are discussed from May, August and September experiments.

In June and July (Table 4) DE temperature solution determined a 17–11% RMSE reduction with respect to AFS but both BE and SUE did not improve this outcome. On June a reduced number of observations, sampled in the northernmost zone, has been assimilated in the IC, making the blending strategy not successful. In July blending initialization technique is again fruitless on temperature field; the error locates below 10m where few station samples exist (Fig. 1b). Intense southeasterly wind in early July (see Fig. 3a and c) causes a sudden drop of temperature, not captured in this region by both LAMI and ECMWF (not shown), and successive fast alternating winds might generate high frequency processes that the model cannot represent in this very shallow region. June DE salinity gives same AFS results while in July DE improves it of a 10%. BE salinity slightly ameliorates in June (5% gain) and highly improves in July (27% gain), correcting a uniform AFS negative bias over the water column. ASHELF May case in Emilia Romagna (Fig. 11a) shows slight improvement for temperature, but the AFS cold bias is still evident at the surface. Salinity profiles exhibit surface bias reduction on the order of 0.5 psu for the DE case and 1 psu for cases BE and SUE but observed surface salinity is still fresher. The validation have been conducted on a reduced number of profiles, 23 instead of 29, where the 6 southernmost stations miss (Fig. 1b), negatively affecting the final score since the northernmost region is where model predictability is worst owing to the vicinity of the Po river delta, especially in May when runoff is abundant (Fig. 2). Furthermore, below 5m the blending procedure (Fig. 5a) could not correct effectively AFS temperature and salinity profiles because of the scarce number of samples reaching this depth. Thus we conclude that the increased realism in the coastline and the runoff for the Po river in ASHELF is not enough to significantly reduce the RMSE. More work is required to simulate the Po river runoff, probably introducing tidal effects and larger river mixing in the delta, as shown in a recent paper by Malacic and Petelin (2009). Moreover daily runoff for the minor rivers and additional monitoring stations far offshore are advisable to further improve CREA outcome that rely on daily time scales. August temperature profiles are in good agreement with observations (Fig. 11b) and the blending or the SUE solution do not differ significantly. Salinity slightly ameliorates in the DE case above 4m depth and below 10m. BE and SUE highly improve salinity sub-surface result but present a 0.5 psu positive bias at the surface. In September only 8 observations were assimilated in the initial condition, however CREA outcome is positive (Fig. 11c). ASHELF surface temperature highly improves thanks to the new light absorption parameterization, but also subsurface values get closer to observations except for the BE case. SUE reduces AFS temperature RMSE of almost a 30%. Salinity ameliorates too reducing AFS surface bias of almost 1 psu. SUE profiles are the closest to observations and reduce AFS salinity RMSE of a 23%. In this case the blending approach produces only a 3–4% improvement respect to the downscaling answer, due to the few profiles assimilated, but with a preliminary spin up period model solution ameliorates up to 15–11%. Between August and September an abrupt cooling (see Fig. 3a and c) due to the increase of wind intensity determines the breakdown of the summer stratification. Two Bora wind (northeasterly wind) events alternate with few days of weak Scirocco (southeasterly wind) that enhance the water column mixing process. ASHELF in this case reproduces better than AFS the water column dynamics.

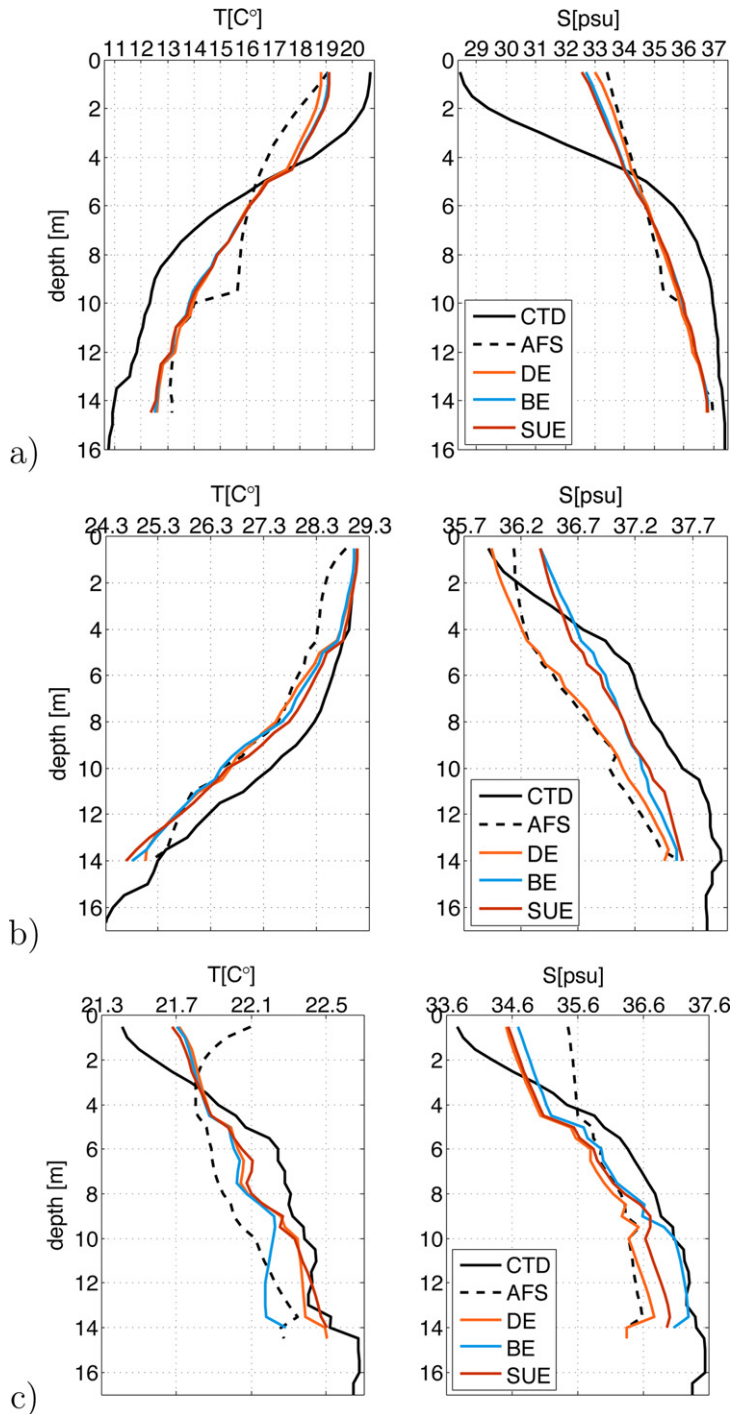


**Fig. 11.** AFS and CREA (DE, BE, SUE) averaged profiles in the Emilia Romagna region from May, August and September experiments, compared to observations (CTD) when available for verification: (a) May 12th; (b) August 18th–19th; (c) September 17–18th. Synthetic profiles have been extracted from ASHELF and AFS models on CTD space–time locations and then averaged.

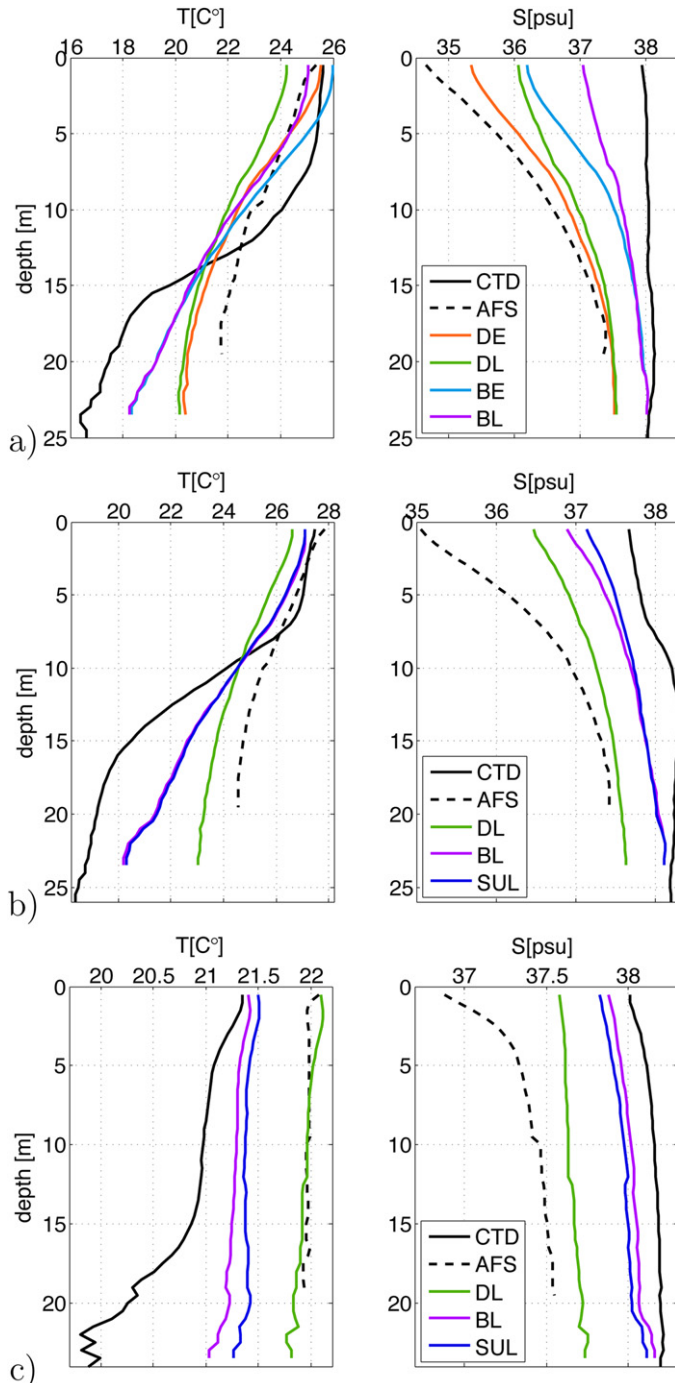


**Fig. 12.** AFS and CREA averaged profiles in the Gulf of Trieste from July (DE, DL, BE, BL), August (DL, BL, SUL) and September (DL, BL, SUL) experiments, compared to observations (CTD) when available for verification: (a) July 14th; (b) August 18th and (c) September 17th. Synthetic profiles have been extracted from ASHELF and AFS models on CTD space-time locations and then averaged.

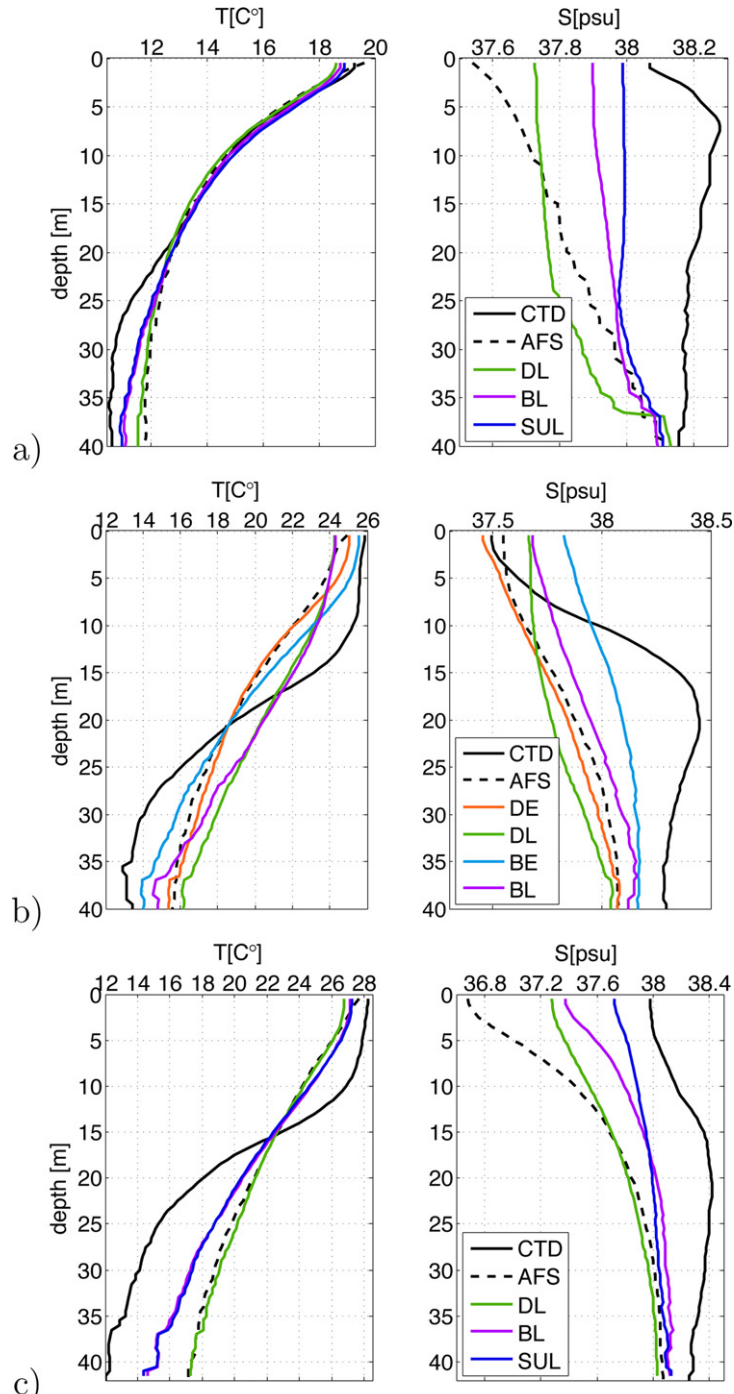


**Fig. 13.** AFS and CREA averaged profiles in the Rovinj coastal area from May (DL, BL, SUL), July (DE, DL, BE, BL) and August (DL, SUL) experiments, compared to observations (CTD) when available for verification: (a) May 13th; (b) July 15th; (c) August 19th. Synthetic profiles have been extracted from ASHELF and AFS models on CTD space-time locations and then averaged.

In the Gulf of Trieste (Table 5) downscaling method slightly ameliorate temperature solution (3% gain) but strongly corrects AFS salinity fields achieving a 19% RMSE reduction with ECMWF forcing and a 38% improvement utilizing LAMI forcing. Blending procedure (*BE*, *BL*) produces a 32–37% temperature gain and a 45–68% salinity gain. An additional spin up period positively affects salinity solution in August and September. Fig. 12 displays CREA solutions for July, August and September cases, when CTD data were available for verification. It must be noticed that AFS averaged profiles ends at 19 m depth while ASHELF ones reach 23 m while observations have been sampled up to 25 m. This region is in fact one of the areas where AFS and ASHELF topographies differ most.

In July (Fig. 12a) *DE*, *DL*, *BE*, *BL* experiments are shown to analyze temperature results when different atmospheric forcing are applied. The Gulf of Trieste presents a pronounced thermal stratification with a thermocline settling at about 15 m depth with an average surface temperature value between 25 and 26 °C and a bottom value of approximately 16.5 °C. AFS totally fails in simulating such thermal stratification. *DE* temperature profiles exhibit a stronger thermal stratification and surface values that are in agreement with observations. *BE* improves temperature solution below the thermocline but not above it, thus rather decreasing model skill. Temperature profiles from *DL* are generally colder than AFS and are closer to the observed profile only below the thermocline. *BL* enhances the vertical stratification but still underestimating surface temperature observations. This confirms ASHELF cold bias recorded by SST field (see Fig. 10c) when LAMI forcing is applied. Observed salinity on contrary is totally unstratified and AFS present a large surface bias that diminishes with depth. *DE* and *DL* strongly reduce AFS bias, with best result when LAMI forcing is applied. Data assimilation (*BE*, *BL*) further improve the results mainly diminishing the surface bias to approximately 1 psu, which is caused by the use of climatological river runoff. Salinity improvement is bigger when LAMI forcing is considered. In August (Fig. 12b) temperature profiles from *DL* are again generally cooler than AFS and are closer to the observed profile below the thermocline. *BL* shows a big improvement enhancing the stratification, almost absent in AFS. Mean temperature gain is 37% even if LAMI reduced the heat flux at the surface. Salinity generally improves in the *DL* case and it further improves for *BL* and *SUL*, reaching a total gain of 70% with respect to AFS performance. In September (Fig. 12c) the water column appears more homogeneous due to the breakdown of the seasonal thermocline. AFS and *DL* present a constant 1 °C bias that *BL* greatly corrects with an RMSE total gain of about a 60%. AFS salinity profile is approximately 1 psu colder than the observed one. *DL* reduces AFS bias but *BL* gets the best results reaching a total gain of 75% with 0.3 psu RMSE.

In Rovinj coastal zone (Table 6) downscaling procedure slightly improves AFS temperature and salinity results with best scores when LAMI forcing is used. Data assimilation is effective reducing ASHELF (*DE*, *DL*) RMSEs of 20–25%. Temperature solution with data assimilation (*BE*, *BL*) gets better when ECMWF data are considered while salinity obtains better results always with LAMI forcing. A preliminary spin up period slightly affects temperature but may further ameliorate salinity outcome. Fig. 13 shows May, July and August CREA results.

*DL* temperature profile almost overlap AFS profile in May (Fig. 13a) except for the surface value which differ due to the different light absorption assumptions. *BL* and *SUL* slightly ameliorate *DL* at the surface and in the bottom layer. While *DL* does not ameliorate AFS salinity solution, *BL* salinity profile shows a significant improvement in the whole water column that further improves in *SUL*. CREA outcome in June (not shown) resembles May one except for the missing spin up improvement on temperature field. In July *DE*, *DL*, *BE*, *BL* profiles are shown to better understand temperature results when the two different atmospheric forcing are applied (Fig. 13b). *DL* improves AFS subsurface temperature values but it remains too cold at the surface. *DE* ameliorate surface temperature values that in *BE* after assimilation matches observations while *BL* solution improves *DL* outcome only below the thermocline, confirming a bad solar radiation estimation when LAMI is used because of its overestimation of cloud cover. *DE* salinity solution resembles AFS solution. Data assimilation in all cases lowers mean RMSEs increasing salinity results below 10 m depth but slightly overestimating it at the surface. In August (Fig. 13c) *DL* reproduces AFS temperature and salinity solution with a small salinity bias reduction within the surface layer. *BL* and *SUL*, as in Trieste case (Fig. 12b), improve the temperature solution, preserving to a certain extent the strong thermal stratification introduced with the *ab* IC. In fact *ab* averaged initial condition profiles (Fig. 6b and c) almost overlap the observed mean profile but after 7 days the CREA (*BL*, *SUL*) averaged profile lost part of the stratification due to excessive mixing.

*BL* salinity profile approaches the observed profile with a general gain in the whole water column that *SUL* solution further advances in the surface layer. As in July ECMWF forcing (see Table 6) gives better temperature results than LAMI at the surface in this region. In September (not shown) ECMWF improve temperature above the thermocline that settles at 20 m depth while LAMI gets better results below it producing on average a larger score. Salinity score is best when LAMI is used.

CREA results show that our initialization technique improves the 7–8 days forecast in the Gulf of Trieste and Rovinj more than in the Emilia-Romagna region. This is probably due to the lack of sampling in the deep part of the water column of the Emilia-Romagna observations but also to missing daily river outflow informations since most of the data are collected very close to local rivers mouths. The larger errors in the bottom layers suggest that even if the IC is corrected by the observations (see Fig. 6b), sometime the information can be lost again during forecast due to dynamical adjustment and evolution (see Fig. 12b). Model error due to excessive mixing or unresolved coastal processes, like tides, might be the causes of losing the IC improvement. Moreover CREA validation after 7–8 of forecast, due to data availability, might have failed to catch CREA major potential improvements. Additional analysis have been performed in order to understand the impact of unresolved processes in the model results. Two different versions of the AFS system (with and without tides, Antonio Guarneri – INGV, personal communication, <http://gnoo.bo.ingv.it/afs/>) have been compared, using the proposed diagnostics, against available observations. The introduction of tides did not ameliorate significantly SST, temperature and salinity results due probably to the kind of validation and the periods considered, however ASHELF will be upgraded including this coastal process in the near future.

The significant improvement of salinity in the Gulf of Trieste (*DE* – *DL* see Table 5) can be understood with changes in the circulation induced by ASHELF. When ASHELF uses ECMWF (*DE*), as AFS, these changes can be mainly related to positive effects induced by a higher resolution topography and new river data that ameliorate the realism of costal environment representation. LAMI forcing produces wind fields with more realistic small scale spatial structure thanks to a better representation of coastal orography (Signell et al., 2005) and this further positively influences ASHELF solution (*DL*) in the Gulf of Trieste. Salinity maps on August 18th (Fig. 14) for AFS (a) and *DL* (b), show different salinity and current patterns after a week of simulation. AFS reproduces the Istrian Counter Current (ICC) consistent with numerical results from Zavatarelli and Pinardi (2003). In AFS (Fig. 14a) the ICC is part of an anti-cyclonic structure which advects fresher waters from the Tagliamento river and Marano/Grado lagoons along the Istrian peninsula. *DL* improves (Fig. 14b) the salinity field since it weakens the anticyclone and does not advect so far southward the river waters. In general LAMI tightens the fresh water front keeping low salinity water closer to the coast.

Coarser ECMWF data provide, on average, the best CREA results given their performance is constant in time and space and thus not dependent on the target period or region. Finer resolution LAMI data present a more variable error, but they are advisable under particular wind regimes and where the coastal orography plays a crucial role in driving the circulation, like in the Gulf of Trieste region.

## 7. Summary and conclusions

A new Marine Rapid Environmental approach, termed CREA, consisting of a nested high-resolution model, ASHELF, together with an initialization procedure that blends observations from opportunity networks and first guess fields from an operational coarser forecasting model, AFS, is evaluated during the summer and spring season of 2003 in the Northern Adriatic coastal areas. The initialization procedure consisted of an interpolation/extrapolation procedure and a blending technique to merge the model fields with observations.

The interpolation/extrapolation procedure, which takes into account the mean water column structure and the ambient stratification, improves on average AFS temperature 7–8 days forecast skills by about 8%, independently by the atmospheric forcing applied. AFS salinity skills improves by a 9% when ECMWF forcing is used and by a 16% when LAMI is applied because it narrows the fresh water front keeping low salinity water closer to the coast. A small effect of LAMI precipitations might have slightly influenced the salinity fields positively. ASHELF SST ameliorates AFS solution by a 8% (Table 3) when forced by ECMWF, while it gets worst on average with LAMI owing to its frequent overestimation of

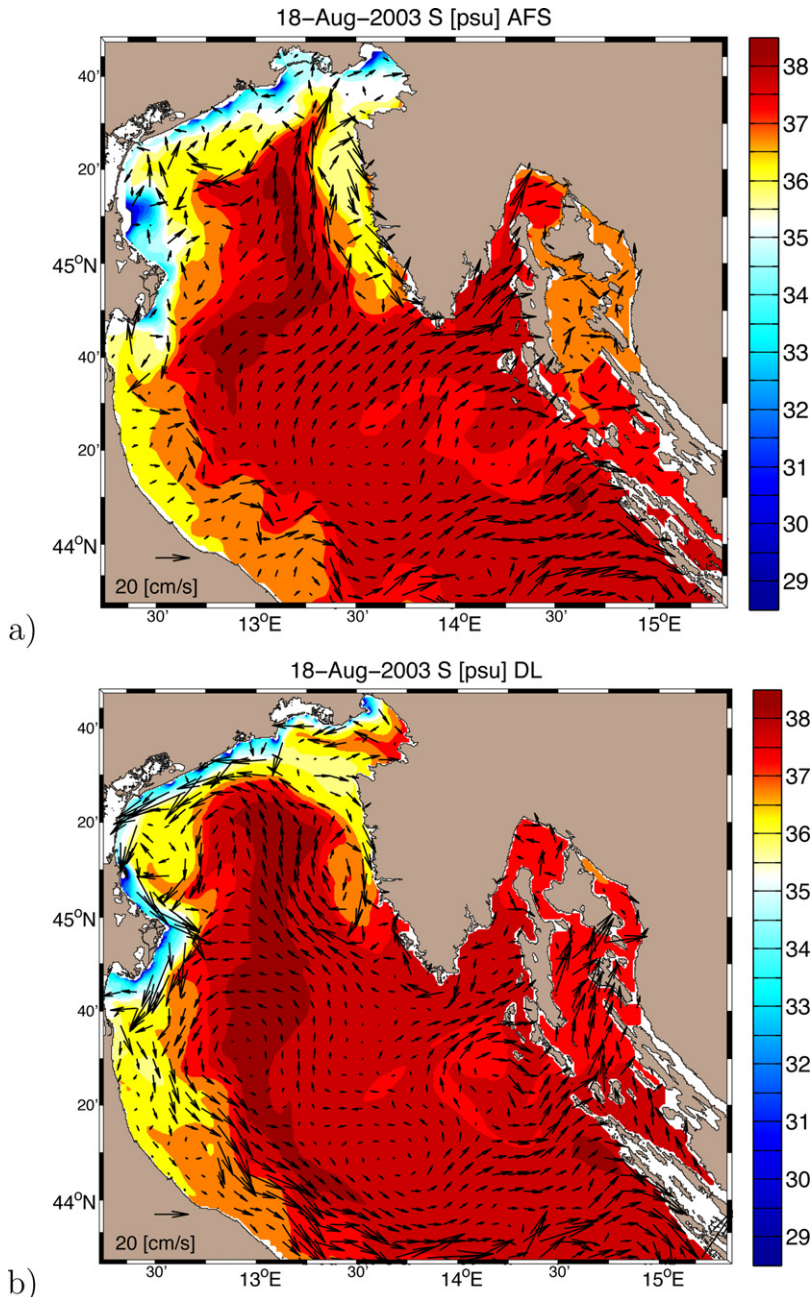


**Fig. 14.** Model results from the August CREA experiment starting August 11th. Daily mean salinity and currents for August 18th: (a) AFS and (b) ASHELF (DL) forced by LAMI.

cloud cover field, that badly influences solar radiation component of surface heat flux cooling to much SST already lowered with respect to AFS by the new ASHELF light absorption parameterization.

The blending initialization technique, based on Mariano and Brown (1992) OI scheme was effective in correcting AFS initial fields with coastal observations and the resulting predicted temperature error is lower than AFS by 25% while salinity error by 28–35% with bigger improvement when LAMI is applied. SST results do not significantly ameliorate after coastal data assimilation since surface observations samples at 0.5–1 m depth and may differ from temperature sampled by the satellite, especially during the summertime.

Besides interpolation and blending, the effects of spin-up time in the initialization procedure were also evaluated. These experiments indicated the greatest salinity error reduction for a 7 day spin-up period. This error reduction is probably due to the dynamical effect of river runoff in the higher resolution model. The forecast salinity improvement in the spin-up initialization plus blending case with respect to AFS reaches 31–37% with higher gain when LAMI is used. ASHELF SST may experience a 6% beneficial effect (14% of total gain Table 3) from model spin up approach independently from the atmospheric forcing applied while temperature in the coastal areas seems not affected by model spin up because its forcing acts on very high frequency temporal scales. However the spin-up period is extremely sensitive to specific conditions and it should be considered as a tunable parameter.

The Emilia Romagna region is the area where CREA had less success. The reason might be the very high space/time variability that characterizes this very shallow area subject to the direct influence of Po River and the WACC. Here we face a particular “uncertainty cascade” (Ferreira-Coelho and Rixen, 2008) problem where numerical model uncertainty due to unresolved processes (tides, waves) or sub-grid scale noise, sum up with atmospheric forcing uncertainty, the lack of coastal observations and river daily outflow. Another issue in this region is the effectiveness of the sampling scheme which seems not to be optimal for CREA meaning that it should include stations far offshore to better resolve the bottom layer and the transition zone between the WACC and the coastline. The experiments conducted in June and September demonstrated that when a reduced number of observations is assimilated the blending procedure is not as efficient as in the cases of the full monitoring network, reducing the total CREA improvement in RMSE.

The Gulf of Trieste is instead the region where CREA most succeeded with a temperature gain of 37% and a salinity gain of 67% explained by a combination of positive factors like the improved realism of the Gulf representation and new river data (Pasarić, 2004; Malacic and Petelin, 2009) that positively affect the circulation in particular when LAMI higher resolution atmospheric forcing is applied. On top of that an optimal sampling scheme maximizes the initialization procedure outcome in this enclosed area where parent and child model topographies differ most, supplying high frequency informations either missing.

The use of two atmospheric forcing data at different spatial and temporal resolution highlighted the need of high resolution wind to enhance coastal dynamics representation that always positively affects salinity results and temperature where coastal orography plays a fundamental role, like in the Gulf of Trieste. Otherwise the coarse resolution ECMWF forcing determines more accurate heat fluxes that give the best SST results and compensate on coastal temperature fields the lack of high frequency representation. In conclusion the choice of the atmospheric forcing to use should depend on the particular wind regime or the region under investigation. However in a near real time CREA approach the analysis with both higher and coarser resolution forcing is advisable to take into account all possible scenarios.

This work assessed the predictive capabilities of high-resolution models, nested in coarser operational models using environmental protection agency data in the coastal strip. The main conclusion is that nesting in these areas necessitates of the observations to fill the gap between the coarse resolution model and the coastal areas of interest, introducing smaller scale and high frequency informations in the fine resolution model initial condition, in order to add skill to short and medium range forecasts. The gap, due principally to a lack of realism of the AFS operational model in representing the coastal environment, increased introducing a high resolution topography and reducing the minimum depth of the model from 10 to 5 meters. Observations were though necessary to enlarge the field where AFS model did not have solution and produce a better skill with respect to the downscaling approach that simply extrapolate it on the base of the mean water column structure. ASHELF model, in a downscal-

ing approach, has been proven to better represent the coastal dynamics resolving the mesoscale and always ameliorating AFS skill. ASHELF, using the blending approach, propagates further in time the improvement obtained by assimilating coastal observations in the initial condition. CREA validation after 7–8 days of forecast, due to data availability, failed to detect the major potential improvements that should reside within 2–3 days owing to model physics problems that overcome the initial condition advantage, in particular due to excessive mixing. Future development might include tides in ASHELF model and consider the assimilation of current velocity observations and satellite data.

## Acknowledgments

This work was supported by the European Commission MyOcean Project (SPA.2007.1.1.01, development of upgrade capabilities for existing GMES fast-track services and related operational services, grant agreement 218812-1-FP7-SPACE 2007-1). It is dedicated to the life long work of Prof. A.R.Robinson who started the Rapid Environmental Assessment work in the world ocean.

We thank Edward Ryan (RSMAS-MPO, University of Miami) for the fruitful collaboration, Luca Giacomelli (SINCEM Laboratory – University of Bologna) for his technical support, Jacopo Chiggiato and Enrico Minguzzi (ARPA-SIMC Emilia Romagna), Simone Colella (GOS ISAC CNR, RComa) and Giulio Notarstefano (OGS, Trieste), Antonio Guarneri (INGV, Bologna) for providing data. We acknowledge also the hydrologic section of ARPA-SIMC Emilia Romagna that provided Po River data.

A sincere gratitude to all MPO division at RSMAS, University of Miami in particular to: Professor William Johns, Guilherme Castelao, Marcello G. Magaldi, Annalisa Griffa and Angelique Haza.

## Appendix A. Northern Adriatic river data

River discharge data considered in ASHELF has been extracted from different climatological data sets. Most of the Italian rivers data comes from [Raicich \(1994\)](#), except for Isonzo that together with Dragonia and Mirna, have been taken from [Malacic and Petelin \(2009\)](#). Croatian rivers data are from [Pasarić \(2004\)](#). [Table A.7](#) lists the fresh water source points defined in ASHELF model and their relative outflow in m<sup>3</sup>/s. [Raicich \(1994\)](#) data set comprehends many outflow rates grouped according to the location of hydrologic basins like some Italian northern coast rivers originating from the Alps or some eastern coast rivers rising from the Apennines. River discharge in the coastal area between Marecchia and Tronto (not included) minus Foglia has been divided between Marecchia and the main hydrographic basins in the Marche Region (Tesino, Aso, Ete Vivo, Tenna, Chienti, Potenza, Musone, Esino, Misa, Cesano, Metauro) to define Marecchia flow rate. The discharge estimated into the plain between Po and Marecchia has been divided between rivers Uso, Rubicone, Bevano, Po di Volano. Canal Bianco outflow rate has not been changed but its name has been changed in Po di Levante because this is the name of the last part of the river. None fresh water source has been positioned in the plain between Adige and Po and between Adige and Brenta except these last two rivers. Bacchiglione and Agno-Guà flow into the Brenta river before reaching the sea so their runoff has not been considered. Plain between Piave and Brenta corresponds to the hydrographic basin ending into the Venice Lagoon, so the monthly flow has been divided between the three main lagoon outlets: Porto di Chioggia, Porto di Malamocco, Porto di Lido. In the plain between Tagliamento and Piave the outflow has been divided between two main rivers beyond Livenza and Sile: Canale Necessolo, and Canale dei Lovi. Plain between Isonzo and Tagliamento is characterized by resurgent rivers flowing into the Marano and Grado Lagoons and the most important are Stella, Zellina, Aussa. The estimated outflow of the plain plus the outflow of Stella river has been divided between the main lagoon outlets: Porto di Lignano, Zellina, Porto Buso, Canale di Morgo, La Fusa, Bocca di Primero.

None detailed information on eastern coast rivers is available in [Raicich \(1994\)](#) since climatologies in greater part of Eastern Adriatic were based on indirect estimates with evenly distributed inflow along the coast. Croatian rivers (Rasa, Rjecina, Dubracina) data comes from [Pasarić \(2004\)](#) monthly climatologies estimated from data covering the period 1947–2000.

**Table A.7**ASHELF Rivers and monthly climatological outflow in m<sup>3</sup>/s.

River	January	February	March	April	May	June	July	August	September	October	November	December
Foglia	10.8	18.0	12.5	9.3	7.	62.9	0.8	0.33	2.0	3.1	10.0	12.8
Marecchia	12.3	19.2	16.3	14.4	12.1	5.8	2.5	1.7	2.8	4.3	9.5	13.9
Uso	8.0	10.5	11.0	8.0	5.5	2.2	1.3	1.0	1.5	4.3	9.3	9.5
Rubicone	8.0	10.5	11.0	8.0	5.5	2.2	1.3	1.0	1.5	4.3	9.3	9.5
Savio	17.0	25.3	21.3	15.7	11.7	5.3	1.7	1.3	3.0	6.7	15.7	20.0
Bevano	8.0	10.5	11.0	8.0	5.5	2.2	1.3	1.0	1.5	4.3	9.3	9.5
Fiumi Uniti	17.0	25.3	21.3	15.7	11.7	5.3	1.7	1.3	3.0	6.7	15.7	20.0
Lamone	17.0	25.3	21.3	15.7	11.7	5.3	1.7	1.3	3.0	6.7	15.7	20.0
Reno	66	86	90	65	44	23	10	8	12	35	75	78
Po di Volano	8.0	10.5	11.0	8.0	5.5	2.2	1.3	1.0	1.5	4.3	9.3	9.5
Po	1597	1285	1283	1298	2179	1753	1113	697	1443	2102	2436	1906
Po di Levante	22.0	20.0	13.0	15.0	17.0	21.0	16.0	18.0	29.0	33.0	29.0	27.0
Adige	147.0	135.0	148.0	185.0	243.0	346.0	261.0	215.0	239.0	214.0	224.0	182.0
Brenta	73.0	61.0	78.0	137.0	104.0	105.0	64.0	44.0	81.0	104.0	145.0	122.0
Porto di Chioggia	10.7	9.7	16.0	22.3	16.3	21.0	17.0	10.7	17.3	20.0	27.0	19.3
Porto di Malamocco	10.7	9.7	16.0	22.3	16.3	21.0	17.0	10.7	17.3	20.0	27.0	19.3
Porto di Lido	10.7	9.7	16.0	22.3	16.3	21.0	17.0	10.7	17.3	20.0	27.0	19.3
Sile	52.0	48.0	48.0	47.0	50.0	56.0	55.0	54.0	56.0	56.0	57.0	56.0
Piave	5.0	0.0	25.0	53.0	70.0	90.0	61.0	41.0	59.0	71.0	117.0	60.0
Livenza	103.0	86.0	84.0	91.0	77.0	80.0	74.0	63.0	81.0	87.0	117.0	117.0
Canale Nicessolo	14.0	13.0	21.0	29.5	21.5	27.0	22.0	14.0	23.0	26.5	35.5	25.5
Canale dei Lovi	14.0	13.0	21.0	29.5	21.5	27.0	22.0	14.0	23.0	26.5	35.5	25.5
Tagliamento	42.0	20.0	60.0	93.0	92.0	105.0	91.0	93.0	122.0	149.0	180.0	116.0
Porto Lignano	9.6	8.1	9.5	11.5	9.5	10.3	9.6	10.0	10.8	11.2	12.0	11.3
Zellina	9.6	8.1	9.5	11.5	9.5	10.3	9.6	10.0	10.8	11.2	12.0	11.3
Porto Buso	9.6	8.1	9.5	11.5	9.5	10.3	9.6	10.0	10.8	11.2	12.0	11.3
Canale di Morgo	9.6	8.1	9.5	11.5	9.5	10.3	9.6	10.0	10.8	11.2	12.0	11.3
La Fosa	9.6	8.1	9.5	11.5	9.5	10.3	9.6	10.0	10.8	11.2	12.0	11.3
Bocca di Primero	9.6	8.1	9.5	11.5	9.5	10.3	9.6	10.0	10.8	11.2	12.0	11.3
Isonzo	101.0	92.0	105.0	137.0	129.0	118.0	80.0	63.0	91.0	127.0	160.0	121.0
Dragonja	1.5	1.5	1.4	1.5	1.3	0.5	0.2	0.1	0.2	1.5	1.8	1.6
Mirna	10.6	9.7	8.7	9.4	6.1	4.9	1.9	2.1	4.2	7.7	11.4	10.4
Rasa	2.4	2.3	1.8	1.8	1.1	0.6	0.33	0.33	0.8	1.4	2.5	2.1
Rjecina	7.2	7.0	6.3	8.5	6.9	3.2	2.1	1.0	5.1	8.6	12.4	12.8
Dubracina	6.1	4.3	3.4	3.1	3.0	2.3	1.5	1.3	2.5	4.7	6.1	6.8

**Table A.8**

Po River runoff breakdown between the five main mouths in % as a function of the mean total discharge,  $R$  in  $\text{m}^3/\text{s}$  at Pontelagoscuro station, upstream of the Delta.

$R$	Tolle	Pila	Maistra	Gnocca	Goro
1000	12.6	56.5	4.4	16.3	10.2
3000	17.2	52.9	4.3	17.6	8.0
4000	13.0	52.7	4.2	17.9	12.2
6000	12.5	52.8	4.9	17.9	11.9

## References

- Artegiani, A., Bregant, D., Paschini, E., Pinardi, N., Raicich, F., Russo, A., 1997. The Adriatic Sea general circulation. Part I: air sea interactions and water mass structure. *Journal of Physical Oceanography* 27, 1492–1514.
- Bergamasco, A., Gacic, M., 1996. Baroclinic response of the Adriatic Sea to an episode of bora wind. *Journal of Physical Oceanography* 26, 1354–1369.
- Blumberg, A., Mellor, G., 1987. A description of a three-dimensional coastal ocean circulation model. In: Heaps, N.S. (Ed.), *Three-Dimensional Coastal Ocean Circulation Models*. American Geophysical Union, Washington, DC.
- Bretherton, F., Davis, R., Fandry, C.B., 1976. A technique for objective analysis and design of oceanographic experiments applied to mode-73. *Deep Sea Research* 30, 985–1002.
- Castellari, S., Pinardi, N., Coluccelli, A., 2006. The ADRICOSM Pilot Project: a coastal and river Basin prediction system for the Adriatic Sea. *Acta Adriatica* 47, 5–18.
- Celio, M., Malacic, V., Bussani, A., Cermelj, B., Cominci, C., Petelin, B., 2006. The coastal scale observing system component of ADRICOSM: Gulf of trieste network. *Acta Adriatica* 47, 65–79.
- Estubier, A., Levy, M., 2000. Quel schma numrique pour le transport d'organismes biologiques par la circulation ocanique. Tech. rep., Ple de modlisation, Institut Pierre-Simon Laplace.
- Ferreira-Coelho, E., Rixen, M., 2008. Maritime rapid environmental assessment new trends in operational oceanography. *Journal of Marine Systems* 69 (1–2).
- Gabersek, S., Sorgente, R., Natale, S., Ribotti, A., Olita, A., Astraldi, M., Borghini, M., 2007. The Sicily Channel Regional Model forecasting system: initial boundary conditions sensitivity and case study evaluation. *Ocean Science* 33.
- Grbec, B., Vilibic, I., Bajic, A., Morovic, M., Bec Paklar, G., Matic, F., Dadić, V., 2007. Response of the adriatic sea to the atmospheric anomaly in 2003. *Annales Geophysicae* 25 (4), 835–846.
- Guarnieri, A., Oddo, P., Bortoluzzi, G., Pastore, M., Pinardi, N., Ravaioli, M., 2009. The Adriatic Basin forecasting system new model and system development. *Coastal to global operational oceanography: achievements and challenges*. In: Dahlin, H., Fleming, N., Petersson, S. (Eds.), *Proceeding of 5th EuroGOOS Conference*. Exeter, UK.
- Inoue, H., 1986. A least-squares smooth fitting for irregularly spaced data: finite-element approach using the cubic b-spline basis. *Geophysics* 51, 2051–2066.
- Jeffries, M., Lee, C., 2007. A climatology of the northern Adriatic Sea's response to bora and river forcing. *Journal of Geophysical Research* 112.
- Jerlov, N., 1976. *Marine Optics*. Elsevier Sci. Pub. Co.
- Legates, D., Willmott, C., 1990. Mean seasonal and spatial variability in gauge-corrected, global precipitation. *International Journal of Climatology* 10, 111–127.
- Lyons, D.M., Supic, N., Smidkla, N., 2003. Geostrophic circulation patterns in the northeastern Adriatic Sea and the effects of air-sea coupling: May–September. *Journal of Geophysical Research* 112, C03S08.
- Malacic, V., Petelin, B., 2009. Climatic circulation in the gulf of trieste (northern Adriatic). *Journal of Geophysical Research* 114.
- Mariano, A., Brown, O., 1992. Efficient objective analysis of dynamically heterogeneous and nonstationary fields via the parameter matrix. *Deep Sea Research* 39 (7/8), 1255–1271.
- Masina, S., Pinardi, N., 1994. Mesoscale data assimilation studies in the middle adriatic sea. *Continental Shelf Research* 14 (12), 1293–1310.
- Mellor, G.L., Ezer, T., Oey, L.Y., 1994. The pressure gradient conundrum of sigma coordinate ocean models. *Journal of Atmospheric and Oceanic Technology* 11 (4), 1126–1134.
- Mellor, G.L., Oey, L.-Y., Ezer, T., 1998. Sigma coordinate pressure gradient errors and the seamount problem. *Journal of Atmospheric and Oceanic Technology* 15 (5), 1122–1131.
- Notarstefano, G., Mauri, E., Poulaing, P., 2006. Near surface structure and surface diurnal warming in the Adriatic Sea using satellite and drifter data. *Remote Sensing of Environment* 101, 194–211.
- Oddo, P., Adani, M., Pinardi, N., Fratianni, C., Tonani, M., Pettenuzzo, D., 2009. A nested Atlantic-Mediterranean Sea general circulation model for operational forecasting. *Ocean Science*, 461–473.
- Oddo, P., Pinardi, N., 2008. Lateral open boundary conditions for nested limited area models: a scale selective approach. *Ocean Modeling*, 134–156.
- Oddo, P., Pinardi, N., Zavatarelli, M., 2005. A numerical study of the interannual variability of the Adriatic Sea (2000–2002). *Science of the Total Environment*, 39–56.
- Oddo, P., Pinardi, N., Zavatarelli, M., Coluccelli, A., 2006. The Adriatic basin forecasting system. *Acta Adriatica*.
- Olita, A., Sorgente, R., Natale, S., Gabersek, S., Ribotti, A., Bonanno, A., Patti, B., 2007. Effects of the 2003 European heatwave on the Central Mediterranean Sea: surface fluxes and the dynamical response. *Ocean Science*, 273–289.
- Orlanski, I., 1976. A simple boundary condition for unbounded hyperbolic flows. *Journal of Computational Physics* 21, 251–269.
- Pasarić, M., 2004. Annual cycle of river discharge along the Adriatic coast of Croatia. In: 37th Congress, Proceedings, vol. 37 .. CIESM.

- Paschini, E., Artegiani, A., Pinardi, N., 1993. The mesoscale eddy field of the middle adriatic sea during fall 1988. Deep Sea Research Part I: Oceanographic Research Papers 40 (7), 1365–1377.
- Paulson, C., Simpson, J., 1977. Irradiance measurements in the upper ocean. Journal of Physical Oceanography 7, 952–956.
- Pinardi, N., Allen, I., Demirov, E.P., De Mey, G.K., Lascaratos, A., Traon, P.-Y.L., Maillard, C., Manzella, G., Tziavos, C., 1998. The Mediterranean ocean forecasting system: first phase of implementation (1998–2001). Annales Geophysicae 21, 413–436.
- Pinardi, N., Auclair, F., Cesarin, C., Demirov, E., Umani, S.F., Giani, M., Montanari, G., Oddo, P., Tonani, M., Zavatarelli, M., 2002. Toward Marine environmental prediction in the Mediterranean Sea coastal areas: a monitoring approach. In: Pinardi, N., Woods, J. (Eds.), Ocean Forecasting: Conceptual Basis and Applications. Springer Verlag (Chapter 17).
- Raicich, F., 1994. Note on the flow rates of the Adriatic rivers. Tech. rep., Consiglio Nazionale delle Ricerche, Istituto Sperimentale Talassografico.
- Robinson, A., 1996. Physical processes, field estimation and an approach to interdisciplinary ocean modeling. Earth-Science Reviews 40 (1–2), 3–54.
- Robinson, A., 1999. Forecasting and simulating coastal ocean processes and variabilities with the harvard ocean prediction system. In: Mooers, C. (Ed.), Coastal Ocean Prediction. No. 56 in Coastal and Estuarine Studies Series. American Geophysical Union, pp. 77–100.
- Robinson, A., 2002. Rapid assessment of the coastal ocean environment. In: Pinardi, N., Woods, J. (Eds.), Ocean Forecasting: Conceptual Basis and Applications. Springer Verlag (Chapter 11).
- Signell, R., Carniel, S., Cavalieri, L., Chiggiato, J., Doyle, J., Pullen, J., Sclavo, M., 2005. Assessment of wind quality for oceanographic modeling in semi-enclosed basins. Journal of Marine Systems 53, 217–233.
- Smagorinsky, J., 1993. Some historical remarks on the use of non-linear viscosities. In: Large Eddy Simulations of Complex Engineering and Geophysical Flows. Cambridge University Press, pp. 3–36.
- Tonani, M., Pinardi, N., Dobricic, S., Pujol, I., Fratianni, C., 2008. A high resolution free-surface model of the Mediterranean Sea. Ocean Science, 1–14.
- Zavatarelli, M., Pinardi, N., 2003. The Adriatic Sea modeling system: a nested approach. Annales Geophysicae, 345–364.